

Analysis of Collective Neutrino Flavor Transformation in Supernovae

Huaiyu Duan* and George M. Fuller†

Department of Physics, University of California, San Diego, La Jolla, CA 92093-0319

J. Carlson‡

Theoretical Division, Los Alamos National Laboratory, Los Alamos, NM 87545

Yong-Zhong Qian§

School of Physics and Astronomy, University of Minnesota, Minneapolis, MN 55455

(Dated: October 13, 2018)

We study the flavor evolution of a dense gas initially consisting of pure mono-energetic ν_e and $\bar{\nu}_e$. Using adiabatic invariants and the special symmetry in such a system we are able to calculate the flavor evolution of the neutrino gas for the cases with slowly decreasing neutrino number densities. These calculations give new insights into the results of recent large-scale numerical simulations of neutrino flavor transformation in supernovae. For example, our calculations reveal the existence of what we term the “collective precession mode”. Our analyses suggest that neutrinos which travel on intersecting trajectories subject to destructive quantum interference nevertheless can be in this mode. This mode can result in sharp transitions in the final energy-dependent neutrino survival probabilities across all trajectories, a feature seen in the numerical simulations. Moreover, this transition is qualitatively different for the normal and inverted neutrino mass hierarchies. Exploiting this difference, the neutrino signals from a future galactic supernova can potentially be used to determine the actual neutrino mass hierarchy.

PACS numbers: 14.60.Pq, 97.60.Bw

I. INTRODUCTION

In this paper we employ physical, analytic insights along with the results of large-scale numerical calculations to study the nature of collective neutrino and antineutrino flavor transformation in supernovae. Although neutrino flavor transformation is an experimental fact, modeling this process in astrophysical settings can be problematic. In part, this is because nature produces environments where the number densities of neutrinos and/or antineutrinos can be very large. Examples of these include the early universe and environments associated with compact-object mergers and gravitational collapse. In particular, core-collapse supernovae result in hot proto-neutron stars that emit neutrinos and antineutrinos copiously from the neutrino sphere. This implies inhomogeneous, anisotropic distributions for these particles. As their trajectories intersect above the proto-neutron star, their flavor evolution histories are quantum mechanically coupled [1]. The flavor content of the neutrino and antineutrino fields in and above a proto-neutron star will be a necessary ingredient for the interpretation of neutrino signals from a future supernova. It can also be an important, even crucial determinant of the composition of supernova ejecta [2] and possibly even the supernova explosion mechanism [3]. Consequently, if

we are to understand core-collapse supernovae, it follows that we must understand neutrino and antineutrino flavor evolution in them.

Large neutrino number densities imply that neutrino-neutrino in addition to neutrino-electron forward scattering sets the potential which governs neutrino flavor conversion. Because of the neutrino-neutrino forward scattering potential [4–6], neutrino flavor transformation in the early universe and near the supernova core can be very different from that in the vacuum or in an ordinary matter background only [7–17]. Recent analytical and numerical studies have revealed a new paradigm for neutrino flavor transformation in supernovae [18–26], one which is completely different from vacuum oscillations or the conventional Mikheyev-Smirnov-Wolfenstein (MSW) mechanism [27–29].

A particular aspect of this new paradigm is best discussed in the following framework: The 2×2 neutrino flavor transformation problem can be described as the motion of isospins in flavor space, wherein $\nu_e/\bar{\nu}_{\mu,\tau}$ and $\bar{\nu}_e/\nu_{\mu,\tau}$ correspond to the “up” and “down” states of these isospins [21]. Both analytical and numerical studies have suggested that a dense neutrino gas originally in a “bipolar configuration” (*i.e.*, with the corresponding neutrino flavor isospins or NFIS’s forming two oppositely oriented groups) tends to stay in such a configuration even though each isospin group is composed of neutrinos and/or antineutrinos with finite energy spread. In other words, neutrinos and antineutrinos with different energies can experience collective flavor transformation at high neutrino number densities. This is very different from the conventional MSW paradigm in which neutrinos

*Electronic address: hduan@ucsd.edu

†Electronic address: gfuller@ucsd.edu

‡Electronic address: carlson@lanl.gov

§Electronic address: qian@physics.umn.edu

and antineutrinos with different energies undergo flavor transformation independently.

A neutrino system with a bipolar configuration is also referred to as a “bipolar system”. Because supernova neutrinos are essentially in their flavor eigenstates when they leave the neutrino sphere, they naturally form a bipolar system. The neutrino sphere is in the very high density, electron degenerate environment near the neutron star surface.

For a simple bipolar system consisting of mono-energetic ν_e and $\bar{\nu}_e$ initially, it has been shown that the evolution of the system is equivalent to the motion of a (gyroscopic) pendulum [24]. Therefore, a bipolar system generally can evolve simultaneously in two different kinds of modes, *i.e.* the precession mode and the nutation mode, in analogy to the mechanical motion of a gyroscopic pendulum. In the extreme limit of large neutrino number density, a bipolar system is reduced to a synchronized system, which is in a pure precession mode characterized by a common synchronization frequency [14]. The evolution of bipolar systems in the presence of an ordinary matter background has been studied in Refs. [21, 24] using corotating frames.

Refs. [22, 23] have presented by far the most sophisticated, large-scale numerical simulations of neutrino flavor transformation in the coherent regime near the supernova core. For example, these simulations for the first time self-consistently treated the evolution of neutrinos propagating along various intersecting trajectories. These simulations clearly show that the conventional MSW paradigm is invalid near the supernova core where neutrino fluxes are large. However, analytical models so far have only corroborated some of the features demonstrated by the simulations, and there are some obvious gaps between the analytical and numerical studies.

One of the gaps is that current analytical models of bipolar systems assume constant neutrino number densities, which is not true in supernovae. Using some simple numerical examples, Ref. [24] has shown that some interesting phenomena observed in the simulations [22, 23] are related to varying neutrino number densities. For example, the energy averaged neutrino survival probabilities change as neutrino number densities decrease with the radius. In this paper we will show that if the neutrino number density decreases slowly as the system evolves out of the synchronized limit at high neutrino densities, the bipolar system will be dominantly in a precession mode. The neutrino flavor evolution seen in the numerical simulations is the combined effect of this precession mode and the nutation modes that are generated as a result of the finite rate of change in neutrino number densities.

Another important gap between analytical and numerical studies is that most of the current analytical models assume homogeneity and isotropy of the neutrino gas, which is not true of the supernova environment. A recent analytical study which assumes an initial state of ν_e and $\bar{\nu}_e$ with equal densities shows that the collec-

tivity (referred to as “coherence” or “kinematic coherence” in Ref. [24]) of the nutation modes tends to break down quickly among different neutrino trajectories in an inhomogeneous and anisotropic environment [26]. However, the numerical simulations presented in Refs. [22, 23] employed more realistic supernova conditions where the initial ν_e and $\bar{\nu}_e$ as well as $\nu_{\mu,\tau}$ and $\bar{\nu}_{\mu,\tau}$ do not have the same number densities. These simulations do show some clear signs of collective flavor transformation. One important example is the hallmark pattern in the final energy-dependent neutrino survival probability which has a sharp transition energy across all neutrino trajectories (Fig. 3 of Ref. [23]). We have further analyzed the numerical results obtained in the large-scale simulations mentioned above and found that, apart from the non-collective nutation modes, neutrinos propagating along different trajectories were in a single, collective precession mode. It is this precession mode that facilitates the mechanism suggested in Ref. [22] for producing the fore-mentioned hallmark pattern in the final neutrino survival probability.

This paper is organized as follows. In Sec. II we will study the properties of a symmetric bipolar system initially consisting of an equal number of ν_e and $\bar{\nu}_e$. We will use an adiabatic invariant of the system to obtain some analytical understanding of the evolution of such a system as neutrino number densities change. In Sec. III we will compare a simple asymmetric bipolar system with a gyroscopic pendulum. We will revisit the criteria determining whether a bipolar system is in the synchronized or bipolar regime and clarify the description of bipolar oscillations. In Sec. IV we will show that an asymmetric bipolar system can stay roughly in a pure precession mode if neutrino number densities decrease slowly. We will also demonstrate some interesting properties of such a precession mode which can explain the results from the simple numerical examples of Ref. [24]. In Sec. V we will apply our simple analytical models to understand the numerical simulations presented in Refs. [22, 23] and offer some new analyses of these simulations. In Sec. VI we give our conclusions.

II. SYMMETRIC BIPOLAR SYSTEM

A. Flavor pendulum

We start with a simple bipolar system initially consisting of mono-energetic ν_e and $\bar{\nu}_e$ with energy E_ν and an equal number density n_ν . Throughout this paper we will assume 2×2 flavor mixing through the active-active channel. According to Ref. [21], the flavor evolution of a neutrino or antineutrino is equivalent to the motion of the corresponding neutrino flavor isospin, or NFIS, in flavor space. For a neutrino, the NFIS in the flavor basis

is defined as

$$\mathbf{s}_\nu \equiv \frac{1}{2} \begin{pmatrix} 2\text{Re}(a_{\nu_e}^* a_{\nu_\tau}) \\ 2\text{Im}(a_{\nu_e}^* a_{\nu_\tau}) \\ |a_{\nu_e}|^2 - |a_{\nu_\tau}|^2 \end{pmatrix}, \quad (1)$$

where a_{ν_e} and a_{ν_τ} are the amplitudes for the neutrino to be in ν_e and another flavor state, say ν_τ , respectively. For an antineutrino, the corresponding NFIS in the flavor basis is

$$\mathbf{s}_{\bar{\nu}} \equiv -\frac{1}{2} \begin{pmatrix} 2\text{Re}(a_{\bar{\nu}_e}^* a_{\bar{\nu}_\tau}^*) \\ 2\text{Im}(a_{\bar{\nu}_e}^* a_{\bar{\nu}_\tau}^*) \\ |a_{\bar{\nu}_e}|^2 - |a_{\bar{\nu}_\tau}|^2 \end{pmatrix}, \quad (2)$$

where $a_{\bar{\nu}_e}$ and $a_{\bar{\nu}_\tau}$ are the amplitudes for the antineutrino to be $\bar{\nu}_e$ and $\bar{\nu}_\tau$, respectively.

To obtain a simple analytical understanding of collective neutrino flavor transformation, we will assume, unless otherwise stated, that the neutrino gas is homogeneous and isotropic and that there is no ordinary matter medium. Using the NFIS notation, the equations of motion (e.o.m.) for the NFIS's \mathbf{s}_1 (neutrino) and \mathbf{s}_2 (antineutrino) of this simple bipolar system are [21]

$$\frac{d}{dt}\mathbf{s}_1 = \mathbf{s}_1 \times (\mu_{V,1}\mathbf{H}_V + \mu_\nu n_{\nu,2}\mathbf{s}_2), \quad (3a)$$

$$\frac{d}{dt}\mathbf{s}_2 = \mathbf{s}_2 \times (\mu_{V,2}\mathbf{H}_V + \mu_\nu n_{\nu,1}\mathbf{s}_1), \quad (3b)$$

and the initial condition is

$$\mathbf{s}_1(0) = -\mathbf{s}_2(0) = \frac{\hat{\mathbf{e}}_z^f}{2}, \quad (4)$$

where

$$n_{\nu,1} = n_{\nu,2} = n_\nu \quad (5)$$

are the number densities of neutrinos and antineutrinos, and $\hat{\mathbf{e}}_z^f$ is the unit vector in the z -direction in the flavor basis. Eq. (3) clearly shows that the motion of the NFIS's is similar to that of magnetic spins. In this “magnetic spin” picture, the “magnetic spins” \mathbf{s}_1 and \mathbf{s}_2 precess around a common “magnetic field”

$$\mathbf{H}_V \equiv -\hat{\mathbf{e}}_x^f \sin 2\theta_v + \hat{\mathbf{e}}_z^f \cos 2\theta_v \quad (6)$$

with “gyro magnetic ratios”

$$\mu_{V,1} = -\mu_{V,2} = \mu_V \equiv \frac{\delta m^2}{2E_\nu}. \quad (7)$$

At the same time, \mathbf{s}_1 and \mathbf{s}_2 are also coupled to each other with a coefficient

$$\mu_\nu \equiv -2\sqrt{2}G_F, \quad (8)$$

where G_F is the Fermi constant.

In this paper we always take the squared difference of the two neutrino vacuum mass eigenvalues to be positive ($\delta m^2 \equiv m_2^2 - m_1^2 > 0$). Accordingly, the vacuum mixing

angle θ_v varies within $(0, \pi/2)$. A normal mass hierarchy corresponds to a mixing angle θ_v with $0 < \theta_v < \pi/4$ and an inverted mass hierarchy corresponds to $\pi/4 < \theta_v < \pi/2$. For an inverted mass hierarchy scenario, we follow Ref. [24] to define

$$\tilde{\theta}_v \equiv \frac{\pi}{2} - \theta_v, \quad (9)$$

which has $0 < \tilde{\theta}_v < \pi/4$. We will loosely refer to both θ_v and $\tilde{\theta}_v$ as vacuum mixing angles.¹

We first look at the scenario with n_ν being constant. With the definition of

$$\mathbf{S}_\pm \equiv n_{\nu,1}\mathbf{s}_1 \pm n_{\nu,2}\mathbf{s}_2, \quad (10)$$

Eqs. (3) and (4) become [21]

$$\frac{d}{dt}\mathbf{S}_+ = \mu_V \mathbf{S}_- \times \mathbf{H}_V, \quad (11a)$$

$$\frac{d}{dt}\mathbf{S}_- = \mu_V \mathbf{S}_+ \times \mathbf{H}_V + \mu_\nu \mathbf{S}_- \times \mathbf{S}_+, \quad (11b)$$

and

$$\mathbf{S}_+(0) = 0, \quad (12a)$$

$$\mathbf{S}_-(0) = n_\nu \hat{\mathbf{e}}_z^f. \quad (12b)$$

It is more convenient to work in the vacuum mass basis where the unit vectors $\hat{\mathbf{e}}_i^v$ are related to those in the flavor basis $\hat{\mathbf{e}}_i^f$ by

$$\hat{\mathbf{e}}_x^v = \hat{\mathbf{e}}_x^f \cos 2\theta_v + \hat{\mathbf{e}}_z^f \sin 2\theta_v, \quad (13a)$$

$$\hat{\mathbf{e}}_y^v = \hat{\mathbf{e}}_y^f, \quad (13b)$$

$$\hat{\mathbf{e}}_z^v = \mathbf{H}_V = -\hat{\mathbf{e}}_x^f \sin 2\theta_v + \hat{\mathbf{e}}_z^f \cos 2\theta_v. \quad (13c)$$

Using Eqs. (11) and (12) one can check explicitly that vector \mathbf{S}_- rotates in the $\hat{\mathbf{e}}_x^v$ - $\hat{\mathbf{e}}_z^v$ plane while \mathbf{S}_+ varies only along the $\hat{\mathbf{e}}_y^v$ -axis [21].

In reality neutrinos can experience collective oscillations only if n_ν is large. The largeness of the neutrino number density in this simple bipolar system is naturally measured by the ratio n_ν/n_ν^0 , where

$$n_\nu^0 \equiv \frac{\mu_V}{|\mu_\nu|} = \frac{\delta m^2}{4\sqrt{2}G_F E_\nu}. \quad (14)$$

¹ Refs. [21–23] have adopted a different convention for the inverted mass hierarchy scenario where $\tilde{\theta}_v$ defined here is the vacuum mixing angle and δm^2 is taken to be negative. We note that these two conventions are equivalent by the simultaneous transformations $|\nu_1\rangle \leftrightarrow |\nu_2\rangle$ and $|\nu_\tau\rangle \rightarrow -|\nu_\tau\rangle$. Correspondingly, one has $\mathbf{H}_V \rightarrow -\mathbf{H}_V$ and $\hat{\mathbf{e}}_{x(y)}^f \rightarrow -\hat{\mathbf{e}}_{x(y)}^f$ in flavor space. The x - and y -components of a NFIS in the flavor basis under these two conventions are different by a sign for the inverted mass hierarchy case.

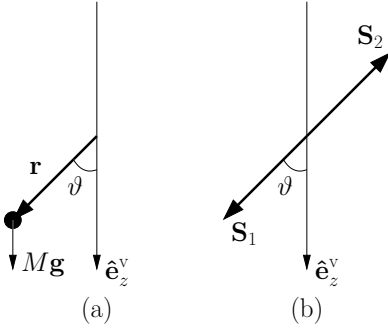


FIG. 1: The equivalence of a pendulum and a symmetric ($n_{\nu,1} = n_{\nu,2} = n_\nu$) bipolar system initially consisting of pure ν_e and $\bar{\nu}_e$. In the limit $n_\nu/n_\nu^0 \gg 1$ two NFIS blocks $\mathbf{S}_1 = n_{\nu,1}\mathbf{s}_1$ (for neutrino) and $\mathbf{S}_2 = n_{\nu,2}\mathbf{s}_2$ (for antineutrino) are always roughly anti-aligned and \mathbf{S}_1 points roughly in the same direction as the pendulum in flavor space.

In the limit $n_\nu/n_\nu^0 \gg 1$, the last term in Eq. (11b) dominates and

$$\frac{d}{dt}\mathbf{S}_- \simeq \mu_\nu \mathbf{S}_- \times \mathbf{S}_+. \quad (11b')$$

Therefore, \mathbf{S}_- roughly maintains a constant magnitude if the neutrino number density is large. As a result, \mathbf{s}_1 and \mathbf{s}_2 are always roughly anti-aligned although their directions can be completely overturned in some scenarios. It is after this special property that “bipolar” flavor transformation was initially named [21].²

We define ϑ as the angle between vectors \mathbf{S}_- and \mathbf{H}_V , which varies within $(0, \pi)$ if $\mathbf{S}_- \cdot \hat{\mathbf{e}}_x^v > 0$ and within $(-\pi, 0)$ if $\mathbf{S}_- \cdot \hat{\mathbf{e}}_x^v < 0$. We also define

$$p_\vartheta \equiv \frac{\mathbf{S}_+ \cdot \hat{\mathbf{e}}_y^v}{n_\nu}. \quad (15)$$

With the initial condition in Eq. (12), we find that Eqs. (11a) and (11b') are equivalent to

$$\dot{p}_\vartheta = -\mu_\nu \sin \vartheta, \quad (16a)$$

$$\dot{\vartheta} \simeq \mu_\nu \left(\frac{n_\nu}{n_\nu^0} \right) p_\vartheta. \quad (16b)$$

Eq. (16) can be further reduced to a differential equation of ϑ of the second order:

$$\ddot{\vartheta} \simeq -\omega^2 \sin \vartheta, \quad (17)$$

where

$$\omega \equiv \mu_\nu \sqrt{\frac{n_\nu}{n_\nu^0}} \quad (18a)$$

$$= \left(\frac{\sqrt{2}G_F \delta m^2 n_\nu}{E_\nu} \right)^{1/2} \quad (18b)$$

is an intrinsic frequency of the system. Because Eq. (17) also describes the motion of a pendulum, we can view the flavor transformation in this simple bipolar system as the motion of a pendulum in the flavor space (Fig. 1). We note that the mass M of the “flavor pendulum” is irrelevant in this case. The only relevant parameter is the ratio between the magnitude of the acceleration field \mathbf{g} and the length of the pendulum r , which is related to the intrinsic frequency by

$$\omega = \sqrt{\frac{g}{r}}. \quad (19)$$

The period of the flavor pendulum is (see, *e.g.*, Ref. [30])

$$T = \frac{4K(\sin(\vartheta_{\max}/2))}{\omega}, \quad (20)$$

where

$$K(k) \equiv \int_0^{\pi/2} \frac{d\zeta}{\sqrt{1 - k^2 \sin^2 \zeta}} \quad (21)$$

is the complete elliptic integral of the first kind [31].

The period of the simple symmetric bipolar system in Eq. (20) takes a simpler form if the vacuum mixing angle θ_v or $\tilde{\theta}_v$ is small. For the normal mass hierarchy scenario with $\theta_v \ll 1$, the pendulum motion is the same as that of a harmonic oscillator and

$$T \simeq \frac{2\pi}{\omega} = 2\pi \left(\frac{E_\nu}{\sqrt{2}G_F \delta m^2 n_\nu} \right)^{1/2}. \quad (22)$$

For the inverted mass hierarchy scenario with $\tilde{\theta}_v \ll 1$, we expand Eq. (20) in terms of $\tilde{\theta}_v$ [31] and find that

$$T \simeq \frac{4 \ln(4/\tilde{\theta}_v)}{\omega} = 4 \ln(4/\tilde{\theta}_v) \left(\frac{E_\nu}{\sqrt{2}G_F \delta m^2 n_\nu} \right)^{1/2}. \quad (23)$$

The period of the bipolar oscillation in this limit has a logarithmic dependence on $\tilde{\theta}_v$ as pointed out in Ref. [24]. The periods of bipolar oscillations calculated using Eqs. (22) and (23) are in excellent agreement with the simple numerical examples in Ref. [21].

Ref. [24] has shown that the evolution of this simple bipolar system is equivalent to a pendulum motion for any n_ν (also see Sec. IIIB). In the limit $n_\nu/n_\nu^0 \gg 1$ the flavor pendulum described here is the same as that in Ref. [24]. This limit is of interest to analyses of the flavor evolution of supernova neutrinos and antineutrinos which have finite spread in their energy distributions, and therefore, may experience the collective flavor transformation only when n_ν is large [21].

² Ref. [24] appears to have misunderstood the origin of the word “bipolar” by stating that the notation “bipolar oscillation” is a “misnomer”.

B. Slowly varying neutrino number density

If the neutrino number density n_ν varies with time, Eq. (3) is still valid but Eq. (11) is not. In this case, Eq. (16) is also valid as long as $n_\nu/n_\nu^0 \gg 1$. We note that ϑ and p_ϑ comprise a canonically conjugate coordinate and momentum pair. In these variables the flavor pendulum has Hamiltonian

$$\mathcal{H} = \mu_V \left[\frac{1}{2} \left(\frac{n_\nu}{n_\nu^0} \right) p_\vartheta^2 - \cos \vartheta \right]. \quad (24)$$

Ref. [24] first noticed that the amplitude of flavor mixing in this bipolar system (or equivalently, the maximal angular position ϑ_{\max} of the flavor pendulum) decreases with the neutrino number density n_ν . Drawing an analogy to the relation between the kinetic energy and the angular momentum of a pirouette performer, Ref. [24] suggested an intuitive explanation for this phenomenon: As n_ν becomes smaller, the effective mass $m_{\text{eff}} \equiv \mu_V^{-1} (n_\nu^0/n_\nu)$ in Eq. (24) increases. As a result, the kinetic energy of the flavor pendulum $E_{\text{kin}} = p_\vartheta^2/(2m_{\text{eff}})$ is reduced with smaller n_ν and the flavor pendulum cannot swing as high as before.

We can arrive at the same conclusion for the scenarios $n_\nu/n_\nu^0 \gg 1$ using Eq. (16). Let us compare the evolution of two flavor pendulums (a) and (b). We assume that the two pendulums have the same values of $(\vartheta, p_\vartheta, \dot{\vartheta}, \dot{p}_\vartheta, n_\nu)$ at instant $t = t_0$. We also assume that pendulum (a) has constant n_ν and that (b) has n_ν decreasing with time. After an infinitesimal interval Δt , both pendulums will have the same values of $(\vartheta, p_\vartheta, \dot{p}_\vartheta)$ but pendulum (b) has smaller $(\dot{\vartheta}, n_\nu)$ than (a) does [see Eq. (16)]. This is equivalent to saying that both pendulums have the same angular position and potential well but pendulum (b) possesses less kinetic energy $E_{\text{kin}} = \dot{\vartheta} p_\vartheta/2$ than (a) does. As a result, pendulum (b) will not swing as high as (a) even if n_ν is constant for $t > t_0 + \Delta t$.

We note that neither Eq. (16) in this paper or Eq. (7) in Ref. [24] is equivalent to the original e.o.m. of the NFIS's [Eq. (3)] if n_ν is small and varies with time. Therefore, this explanation fails for $n_\nu/n_\nu^0 \lesssim 1$.

To quantify the relation between the maximal angular position ϑ_{\max} of the flavor pendulum and the neutrino number density n_ν , we note that in the limit $n_\nu/n_\nu^0 \gg 1$

$$\mathcal{A} \equiv \oint p_\vartheta d\vartheta \quad (25)$$

is an adiabatic invariant of the pendulum motion (see, e.g., Ref. [30]). The integration in Eq. (25) is performed over one pendulum cycle with $-\vartheta_{\max} \leq \vartheta \leq \vartheta_{\max}$. The neutrino number density n_ν is taken to be constant during this cycle.

If n_ν is constant, the Hamiltonian of the flavor pendulum is also a constant and is $-\mu_V \cos \vartheta_{\max}$. Using Eq. (24) we obtain

$$|p_\vartheta| = \sqrt{\frac{2n_\nu^0}{n_\nu}} \sqrt{\cos \vartheta - \cos \vartheta_{\max}}. \quad (26)$$

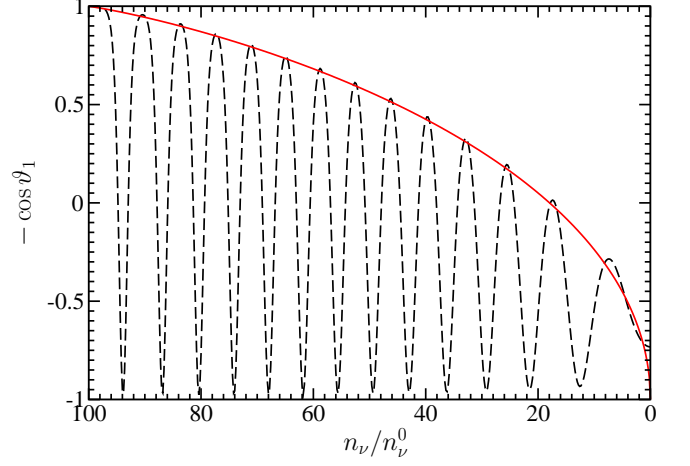


FIG. 2: (Color online) Flavor oscillations of the simple symmetric bipolar system in a nearly adiabatic process [Eq. (34) with $\gamma = 10$ and $n_\nu(0)/n_\nu^0 = 100$] for $\tilde{\theta}_v = 0.01$. The dashed line is the value of $-\cos \vartheta_1$ as a function n_ν computed from Eq. (3) with the initial conditions in Eq. (4). The solid line is $-\cos \vartheta_{\max}$ computed from Eq. (30).

Combining Eqs. (25) and (26) we have

$$\mathcal{A} = -4 \sqrt{\frac{2n_\nu^0}{n_\nu}} \int_{\vartheta_{\max}}^0 \sqrt{\cos \vartheta - \cos \vartheta_{\max}} d\vartheta \quad (27a)$$

$$= 16 \sqrt{\frac{n_\nu^0}{n_\nu}} W(\vartheta_{\max}). \quad (27b)$$

Function $W(\xi)$ in Eq. (27b) is defined as

$$W(\xi) \equiv \frac{1}{2\sqrt{2}} \int_0^\xi \sqrt{\cos \zeta - \cos \xi} d\zeta \quad (28a)$$

$$= \mathbf{E}(\sin(\xi/2)) - \cos^2(\xi/2) \mathbf{K}(\sin(\xi/2)), \quad (28b)$$

where

$$\mathbf{E}(k) \equiv \int_0^{\pi/2} \sqrt{1 - k^2 \sin^2 \zeta} d\zeta \quad (29)$$

is the complete elliptic integral of the second kind [31]. If $n_\nu/n_\nu^0 \gg 1$ and n_ν varies slowly (adiabatic process), then ϑ_{\max} as a function of time satisfies the following relation:

$$W(\vartheta_{\max}) \simeq W(2\theta_v) \sqrt{\frac{n_\nu(t)}{n_\nu(0)}}. \quad (30)$$

An interesting scenario is that $\tilde{\theta}_v = \pi/2 - \theta_v \ll 1$. In this case, $\hat{\mathbf{e}}_z^f \simeq -\mathbf{H}_V$ and the probability for a neutrino to be ν_e is

$$P_{\nu_e \nu_e} = \frac{1}{2} + \mathbf{s}_1 \cdot \hat{\mathbf{e}}_z^f \simeq \frac{1 - \cos \vartheta_1}{2} \lesssim \frac{1 - \cos \vartheta_{\max}}{2}, \quad (31)$$

where ϑ_1 is the angle between the directions of \mathbf{s}_1 and \mathbf{H}_V . Noting that $W(2\theta_v) \simeq W(\pi) = 1$, we find that

$$0 \lesssim P_{\nu_e \nu_e}(t) \leq (P_{\nu_e \nu_e})_{\max}, \quad (32)$$

where

$$(P_{\nu_e \nu_e})_{\max} \simeq \frac{1}{2} \left[1 - \cos \left(W^{-1} \left(\sqrt{\frac{n_\nu(t)}{n_\nu(0)}} \right) \right) \right] \quad (33)$$

is the maximal value that $P_{\nu_e \nu_e}$ may take for a given n_ν . In the above equation $W^{-1}(\xi)$ is the corresponding inverse function of $W(\xi)$.

For a concrete example, we assume that $n_\nu(t)$ has a linear dependence on time t :

$$n_\nu(t) = n_\nu(0)(1 - \gamma^{-1} \mu_V t), \quad (34)$$

where γ is the adiabatic parameter. The larger the value of γ , the more adiabatic the process is. Taking $\hat{\theta}_v = 0.01$, we calculate the value of $-\cos \vartheta_1$ as a function of n_ν for $\gamma = 10$ and $n_\nu(0)/n_\nu^0 = 100$ by solving Eq. (3) with the initial conditions in Eq. (4). The results are plotted as the dashed line in Fig. 2. We have also computed ϑ_{\max} from Eq. (30) and plot $-\cos \vartheta_{\max}$ as the solid line in Fig. 2. It is clear that $-\cos \vartheta_{\max}$ outlines the upper envelope of $-\cos \vartheta_1$ for $n_\nu/n_\nu^0 \gg 1$.

Using the analogy of harmonic oscillators, Ref. [24] has argued that, for the scenario with $\hat{\theta}_v \ll 1$, $(P_{\nu_e \nu_e})_{\max}$ should depend linearly on $\sqrt{n_\nu}$, at least when $\vartheta_{\max} \ll 1$. However, it is clear that this conjecture is not true if ϑ_{\max} is significant. In this case, $(P_{\nu_e \nu_e})_{\max}$ can be understood using the general form of $W(\xi)$ and Eq. (33). On the other hand, we note that

$$W(\vartheta_{\max}) \simeq \frac{\pi}{4} \left(\frac{\vartheta_{\max}}{2} \right)^2 \quad (35)$$

for $\vartheta_{\max} \ll 1$ [31]. Using Eqs. (30) and (35) we obtain

$$\frac{\vartheta_{\max}^2(t)}{\vartheta_{\max}^2(t_0)} \simeq \sqrt{\frac{n_\nu(t)}{n_\nu(t_0)}}, \quad (36)$$

where t_0 is an instant at which $\vartheta_{\max}(t_0) \ll 1$. Because $P_{\nu_e \nu_e} \simeq (1 - \cos \vartheta_1)/2 \simeq \vartheta_1^2/4$, we have

$$(P_{\nu_e \nu_e})_{\max} \simeq \frac{\vartheta_{\max}^2(t_0)}{4} \sqrt{\frac{n_\nu}{n_\nu(t_0)}} \quad (37)$$

for $P_{\nu_e \nu_e} \ll 1$. Therefore, $(P_{\nu_e \nu_e})_{\max}$ does depend linearly on $\sqrt{n_\nu}$ in the limit $\vartheta_{\max} \ll 1$. Note that this result only applies for $n_\nu/n_\nu^0 \gg 1$. As mentioned above, our argument about the adiabatic invariant fails for $n_\nu/n_\nu^0 \lesssim 1$.

III. ASYMMETRIC BIPOLAR SYSTEM

A. Gyroscopic flavor pendulum

We now consider a simple asymmetric bipolar system initially consisting of mono-energetic ν_e and $\bar{\nu}_e$ with

different but constant number densities. We note that Eq. (3) is still valid except that we now take $n_{\nu,1} = n_\nu$ and $n_{\nu,2} = \alpha n_\nu$ with $\alpha \neq 1$ being a positive constant. Ref. [24] has shown that this asymmetric bipolar system is equivalent to a gyroscopic pendulum or a spinning top in flavor space for which

$$\mathbf{S}_+(0) = \frac{1-\alpha}{2} n_\nu \hat{\mathbf{e}}_z^f \quad (38a)$$

$$\mathbf{S}_-(0) = \frac{1+\alpha}{2} n_\nu \hat{\mathbf{e}}_z^f. \quad (38b)$$

To see this we define

$$\mathbf{Q} \equiv \mathbf{S}_- - \frac{\mu_V}{\mu_\nu} \mathbf{H}_V. \quad (39)$$

(Although we follow Ref. [24] in demonstrating the equivalence of an asymmetric bipolar system and a gyroscopic pendulum, we have adopted somewhat different notations for our convenience.) Using Eqs. (11b) and (39) one sees that \mathbf{Q} obeys the e.o.m.

$$\frac{d}{dt} \mathbf{Q} = \mu_\nu \mathbf{Q} \times \mathbf{S}_+ \quad (40)$$

and maintains a constant magnitude

$$Q = n_\nu \left(\frac{1+\alpha}{2} \right) \left[1 + \left(\frac{4}{1+\alpha} \right) \left(\frac{n_\nu^0}{n_\nu} \right) \cos 2\theta_v + \left(\frac{2}{1+\alpha} \right)^2 \left(\frac{n_\nu^0}{n_\nu} \right)^2 \right]^{1/2}. \quad (41)$$

With the definition of

$$\mathbf{J} \equiv \frac{\mathbf{S}_+}{n_\nu}, \quad (42a)$$

$$\mathbf{r} \equiv \frac{\mathbf{Q}}{Q}, \quad (42b)$$

Eqs. (11a), (39) and (40) lead to

$$\dot{\mathbf{J}} = \frac{\mu_V Q}{n_\nu} \mathbf{r} \times \mathbf{H}_V, \quad (43a)$$

$$\dot{\mathbf{r}} = -\mu_V \left(\frac{n_\nu}{n_\nu^0} \right) \mathbf{r} \times \mathbf{J}. \quad (43b)$$

Using Eq. (43) one can easily show that

$$\sigma \equiv \mathbf{J} \cdot \mathbf{r} \quad (44)$$

is a constant of motion. From Eq. (43b) one obtains

$$\mathbf{r} \times \dot{\mathbf{r}} = -\mu_V \left(\frac{n_\nu}{n_\nu^0} \right) (\sigma \mathbf{r} - \mathbf{J}). \quad (45)$$

We note that Eqs. (43a) and (45) are equivalent to

$$\dot{\mathbf{J}} = \mathbf{r} \times M \mathbf{g}, \quad (46a)$$

$$\mathbf{J} = M \mathbf{r} \times \dot{\mathbf{r}} + \sigma \mathbf{r}, \quad (46b)$$

where

$$M = \frac{1}{\mu_V} \left(\frac{n_\nu^0}{n_\nu} \right), \quad (47)$$

$$\mathbf{g} = \frac{\mu_V^2}{n_\nu^0} Q \mathbf{H}_V. \quad (48)$$

Therefore, this asymmetric bipolar system is indeed equivalent to a gyroscopic flavor pendulum. Specifically, \mathbf{r} is the position vector of the bob, \mathbf{J} is the total angular momentum, σ is the internal angular momentum of the bob, M is the mass of the bob, and \mathbf{g} is the acceleration field. The only difference between this pendulum and that shown in Fig. 1(a) is the spin of the bob. Hereafter we will loosely refer to both the symmetric and asymmetric bipolar systems as flavor pendulums.

The motion of the gyroscopic flavor pendulum is the combination of a precession around \mathbf{H}_V and a nutation with $\vartheta_{\min} \leq \vartheta \leq \vartheta_{\max}$. Here ϑ is the polar angle of \mathbf{r} with respect to $\hat{\mathbf{e}}_z^V = \mathbf{H}_V$, and ϑ_{\min} and ϑ_{\max} are the minimal and maximal values of ϑ during nutation. For the simple asymmetric bipolar system that we have discussed, one has $\vartheta_{\max} = \vartheta|_{t=0}$. The value of ϑ_{\min} can be determined as follows. Following Ref. [24] we define the total energy of the pendulum as

$$E_{\text{tot}} = E_{\text{pot}} + E_{\text{kin}} \quad (49a)$$

$$= Mg(1 - \mathbf{H}_V \cdot \mathbf{r}) + \frac{\mathbf{J}^2}{2M} \quad (49b)$$

$$= Mg(1 - \cos \vartheta) + \frac{M\dot{\mathbf{r}}^2}{2} + \frac{\sigma^2}{2M}. \quad (49c)$$

We note that E_{tot} differs from the conserved total effective energy of the NFIS's [21] by only a constant multiplicative factor and an additive constant, and therefore, is also conserved. Because the motion of the pendulum is a pure precession around \mathbf{H}_V when $\vartheta = \vartheta_{\min}$, one has

$$Mg(\cos \vartheta_{\min} - \cos \vartheta_{\max}) = \frac{1}{2} M \sin^2 \vartheta_{\min} \dot{\varphi}^2|_{\vartheta=\vartheta_{\min}}, \quad (50)$$

where φ is the azimuthal angle of \mathbf{r} with respect to \mathbf{H}_V . Using the conservation of the total angular momentum in the direction of the acceleration field \mathbf{g} , one obtains

$$\sigma(\cos \vartheta_{\min} - \cos \vartheta_{\max}) = -M \sin^2 \vartheta_{\min} \dot{\varphi}|_{\vartheta=\vartheta_{\min}}. \quad (51)$$

Combining Eqs. (50) and (51) we have

$$\cos \vartheta_{\min} = -\eta + \sqrt{(\eta + \cos \vartheta_{\max})^2 + (1 - \cos^2 \vartheta_{\max})}, \quad (52)$$

where

$$\eta \equiv \frac{\sigma^2}{4M^2g}. \quad (53)$$

B. Precession/nutation modes and synchronized/bipolar regimes

We shall refer to neutrino flavor transformation as being in the precession (nutation) mode when the corre-

sponding analogous flavor pendulum is undergoing precession (nutation). The symmetric bipolar system discussed in Sec. II corresponds to the limit $\alpha = 1$ and is always in a pure nutation mode. In this limit $\sigma = 0$ and $\vartheta_{\min} = 0$, so the pendulum does not spin at all and simply swings in a fixed plane. Taking $p_\vartheta = \mathbf{J} \cdot \hat{\mathbf{e}}_\vartheta^V$ and ϑ as the angle between \mathbf{r} and \mathbf{H}_V , one can obtain from Eq. (43) that [24]

$$\dot{p}_\vartheta = -\mu_V \left(\frac{Q}{n_\nu} \right) \sin \vartheta \quad (54a)$$

$$\dot{\vartheta} = \mu_V \left(\frac{n_\nu}{n_\nu^0} \right) p_\vartheta. \quad (54b)$$

Eq. (54) is the exact version of Eq. (16). In the limit $n_\nu/n_\nu^0 \gg 1$, $\mathbf{Q} \simeq \mathbf{S}_-$ and \mathbf{S}_- approximately follows a plane pendulum motion as we have discussed in Sec. II A. If the neutrino number density n_ν is constant and the vacuum mixing angle θ_v or $\tilde{\theta}_v$ is small, the bipolar systems in the pure nutation mode can experience almost complete flavor conversion during a nutation period. This is true for various initial configurations (see Table I in Ref. [21]).

A bipolar system generally evolves simultaneously in both precession and nutation modes. However, if the neutrino number density is large enough, it has been shown that a neutrino gas is in the synchronized mode with a characteristic frequency Ω_{sync} independent of its initial configuration [14]. The criterion for synchronization can be written as [21]

$$|\mu_V \mathbf{S}| \gg |\langle \mu_V \rangle|, \quad (55)$$

where

$$\mathbf{S} \equiv \sum_i n_{\nu,i} \mathbf{s}_i \quad (56)$$

is the total NFIS, and

$$\langle \mu_V \rangle \equiv \sum_i \frac{\mu_{V,i} n_{\nu,i} \mathbf{s}_i \cdot \mathbf{S}}{\mathbf{S}^2} = \Omega_{\text{sync}} \quad (57)$$

is the average vacuum oscillation frequency. The index i in Eqs. (56) and (57) denotes neutrinos or antineutrinos with a specific momentum.

For the initial condition in Eq. (38) we note that, if n_ν is large, the total angular momentum of the flavor pendulum is dominated by its spin

$$\mathbf{J} \simeq \sigma \mathbf{r} \quad (58)$$

and

$$\sigma \simeq \frac{1 - \alpha}{2}. \quad (59)$$

In the limit ³

$$n_\nu \gg n_\nu^x \equiv 8 \frac{1+\alpha}{(1-\alpha)^2} n_\nu^0, \quad (60)$$

the parameter η [see Eq. (53)] satisfies $\eta \gg 1$ and

$$\cos \vartheta_{\min} \simeq -\eta + \eta \left(1 + \frac{\cos \vartheta_{\max}}{\eta} \right) \simeq \cos \vartheta_{\max}. \quad (61)$$

As a result, the flavor pendulum roughly maintains a constant latitude and is essentially in the precession mode. One can explicitly show that in this case the flavor pendulum precesses around $-\mathbf{H}_V$ with a constant angular frequency [24]

$$\Omega \simeq \Omega_{\text{sync}} \equiv \frac{1+\alpha}{1-\alpha} \mu_V. \quad (62)$$

Therefore, a bipolar system is synchronized if $n_\nu \gg n_\nu^x$ and the synchronized mode corresponds to a pure precession mode with the synchronization frequency Ω_{sync} as its precession frequency. We refer to the limit in Eq. (60) as the “synchronized regime”. We say that a bipolar system is in the “bipolar regime” if Eq. (60) is not satisfied. In this case it can be in both the precession and nutation modes.

For the simple asymmetric bipolar system discussed here, Eq. (55) lead to

$$n_\nu \gg 2 \frac{1+\alpha}{(1-\alpha)^2} n_\nu^0 = \frac{n_\nu^x}{4}. \quad (63)$$

Eqs. (60) and (63) differ by a constant multiplicative factor. This reflects the fact that there is *no* sharp boundary between the synchronized and bipolar regimes. The simple prescription for the synchronization frequency Ω_{sync} in Eq. (57) allows a ready and practical application of the synchronization condition in Eq. (55) for neutrino and/or antineutrino gases with finite spreads in their energy spectra.

The ways in which the word “bipolar” has been used in the literature [21–24, 26] can be very confusing. There is a tendency to mistakenly identify the synchronized (bipolar) regime with the precession (nutation) mode. This is probably because a flavor pendulum can only precess in the synchronized regime and a symmetric bipolar system was once viewed as a typical bipolar system which is always in a nutation mode. However, the criterion determining whether a bipolar system is mostly in the precession or nutation mode is not the same as that for determining whether it is in the synchronized or bipolar

regime. A good example is that an asymmetric bipolar system can simultaneously be in both the precession and nutation modes in the bipolar regime. We also note that, while the precession frequency Ω of the precession mode in the synchronized regime is determined from Eq. (57) and is independent of the neutrino number density n_ν , the precession frequency of a precession mode in the bipolar regime depends on n_ν (see Sec. IV C).

The evolution of a bipolar system in the bipolar regime is also referred to as bimodal oscillations. Ref. [12] has shown that, in an asymmetric bipolar system initially consisting of mono-energetic ν_e and $\bar{\nu}_e$, the x - and y -components of the polarization vectors of the neutrino and antineutrino ($2\mathbf{s}_1$ and $-2\mathbf{s}_2$ in the NFIS notation) are bimodal as they are functions of two intrinsic periods. It is clear that these two periods are related to the precession and nutation of the flavor pendulum. If ν_e and $\bar{\nu}_e$ have different energies or the system starts with different neutrino/antineutrino species, one can demonstrate that such a system is equivalent to a flavor pendulum in some properly chosen corotating frame [21]. In this case the precession frequency Ω is shifted by the rotation frequency of the corotating frame.

IV. PURE PRECESSION MODE OF ASYMMETRIC BIPOLAR SYSTEMS

A. Pure precession mode

Although a bipolar system tends to develop some nutation in addition to the precession mode in the bipolar regime, the actual mix of these modes depends on the initial conditions as well as the system configuration. For example, a flavor pendulum precesses around $-\mathbf{H}_V$ with constant angular frequency Ω without any nutation if

$$Mg \sin \vartheta = \Omega J_\perp \quad (64a)$$

$$= \Omega (M\Omega \sin \vartheta \cos \vartheta + \sigma \sin \vartheta) \quad (64b)$$

is satisfied, and the corresponding bipolar system is in the pure precession mode. For a gyroscope this is known as the “regular precession”.

With varying neutrino number densities the problem is generally complicated. This is because almost all the parameters of the flavor pendulum (Q , M , g , σ , *etc.*) depend on n_ν and the e.o.m. of a pendulum, Eq. (46), is not equivalent to that of the NFIS’s if $n_\nu(t)$ is not constant. In this case, one has to use Eq. (3) to follow the evolution of the bipolar system. Simple numerical examples presented in Ref. [24] seem to suggest that the evolution of a bipolar system with $\theta_v \simeq \pi/2$ can be dominantly in a precession mode after the system transitions from the synchronized regime into the bipolar regime. Here we try to gain some analytical understanding of this precession mode by using the same simple bipolar system studied in Sec. III but with time-varying n_ν .

We note that, in the synchronized regime (*i.e.*, the limit of large n_ν), both \mathbf{s}_1 and \mathbf{s}_2 precess uniformly

³ Ref. [24] first noticed that the flavor pendulum with $\tilde{\theta}_v \ll 1$ possesses little nutation for $n_\nu \gg n_\nu^x$ and is in the synchronized regime. We note that a flavor pendulum will have little nutation so long as Eq. (60) is satisfied. This result is independent of the value of θ_v .

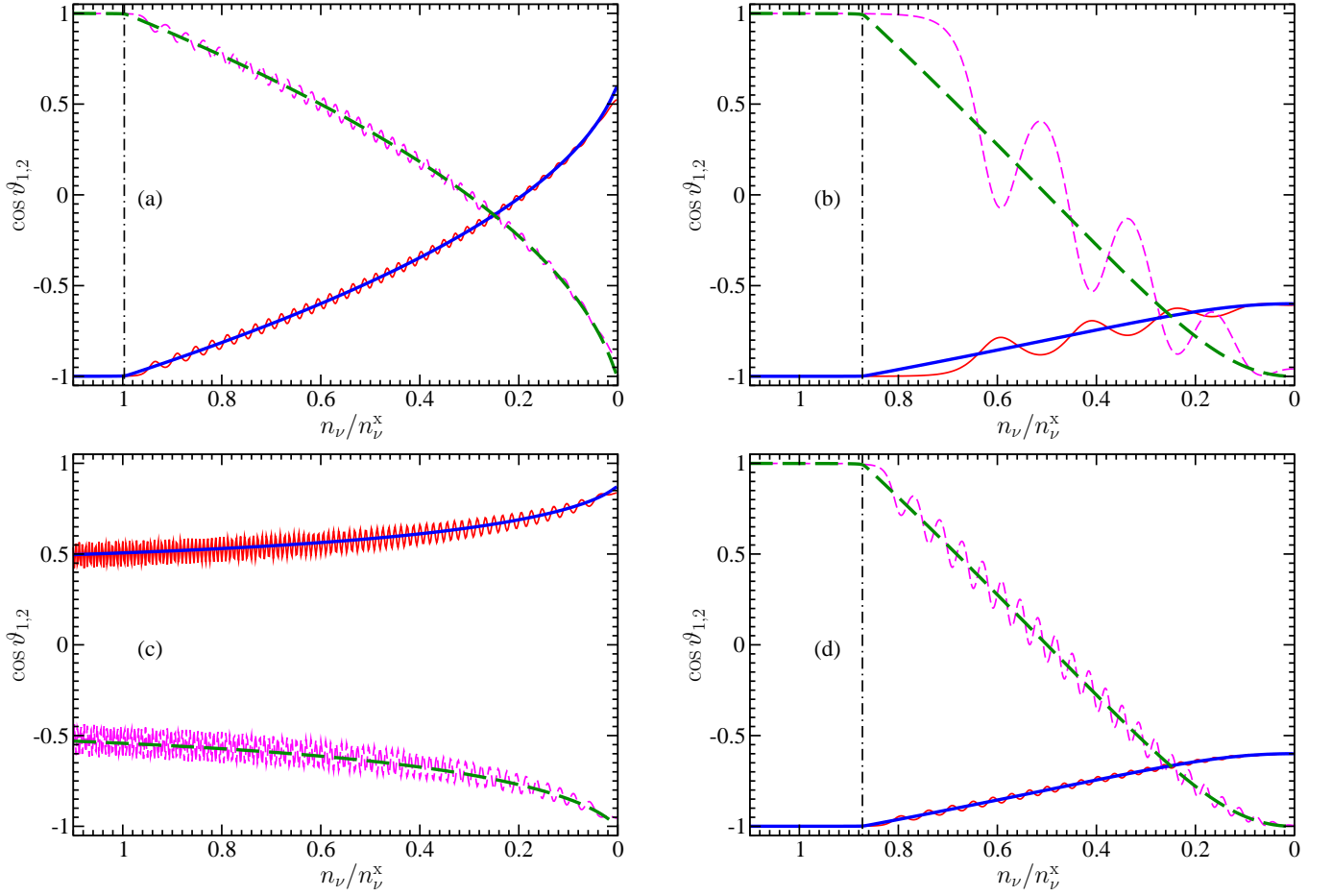


FIG. 3: (Color online) Values of $\cos \vartheta_1$ (solid lines) and $\cos \vartheta_2$ (dashed lines), where ϑ_1 and ϑ_2 are the polar angles of the NFIS's \mathbf{s}_1 and \mathbf{s}_2 with respect to \mathbf{H}_V , as functions of neutrino number density n_ν for simple asymmetric bipolar systems. Panels (a), (b) and (d) have mixing angle $\tilde{\theta}_v = 0.01$ and panel (c) has $\theta_v = 0.6$. The asymmetry parameter is $\alpha = 0.8$ for (a) and (c), and $\alpha = 0.2$ for (b) and (d). The thin lines are computed from the original e.o.m. of NFIS's \mathbf{s}_1 and \mathbf{s}_2 [Eq. (3)] with the initial conditions in (4)] assuming a nearly adiabatic process [Eq. (34) with $n_\nu(0)/n_\nu^x = 2$]. The adiabatic parameter is $\gamma = 40$ for panels (a–c) and is 200 for panel (d). The thick lines are computed from Eq. (66) assuming that bipolar systems stay in the pure precession mode. The vertical dot-dashed lines in panels (a), (b) and (d) correspond to $n_\nu = n_\nu^c$.

around \mathbf{H}_V , and the motion of the NFIS's has a cylindrical symmetry around the axis along \mathbf{H}_V . This symmetry is inherited from the e.o.m. of the NFIS's [Eq. (3)]. We consider an infinitely long process during which n_ν is decreased without preference to any azimuthal angle with respect to \mathbf{H}_V . The cylindrical symmetry in the motion of the NFIS's around \mathbf{H}_V is expected to be preserved in such a process, and \mathbf{s}_1 and \mathbf{s}_2 keep on precessing uniformly around \mathbf{H}_V without any wobbling.

If this is true, vectors \mathbf{s}_1 , \mathbf{s}_2 and \mathbf{H}_V must always be in the same plane, and \mathbf{s}_1 and \mathbf{s}_2 rotates around $-\mathbf{H}_V$ with the same angular frequency

$$\Omega = \mu_V \left[1 - \frac{\alpha}{2 \sin \vartheta_1} \left(\frac{n_\nu}{n_\nu^0} \right) \sin(\vartheta_1 + \vartheta_2) \right] \quad (65a)$$

$$= \mu_V \left[-1 - \frac{1}{2 \sin \vartheta_2} \left(\frac{n_\nu}{n_\nu^0} \right) \sin(\vartheta_1 + \vartheta_2) \right], \quad (65b)$$

where $\vartheta_{1(2)}$ is the angle between $\mathbf{s}_{1(2)}$ and \mathbf{H}_V . On the other hand, from Eq. (3) it can be shown that $\mathbf{H}_V \cdot (\mathbf{s}_1 + \alpha \mathbf{s}_2)$ is time invariant even if n_ν changes with time. Consequently, we obtain the following two equations for ϑ_1 and ϑ_2 :

$$4 \sin \vartheta_1 \sin \vartheta_2 = -\frac{n_\nu}{n_\nu^0} (\sin \vartheta_1 - \alpha \sin \vartheta_2) \times \sin(\vartheta_1 + \vartheta_2), \quad (66a)$$

$$(1 - \alpha) \cos 2\theta_v = \cos \vartheta_1 + \alpha \cos \vartheta_2. \quad (66b)$$

We have solved Eq. (66) numerically for simple asymmetric bipolar systems with different choices of θ_v and asymmetry parameter α . The results are plotted in Fig. 3. For comparison, we have also solved numerically the original e.o.m. of the NFIS's, Eq. (3), for the same bipolar systems assuming that n_ν changes in the way described by Eq. (34). These results are also shown in

Fig. 3. Clearly, the polar angles ϑ_1 and ϑ_2 of the NFIS's \mathbf{s}_1 and \mathbf{s}_2 oscillate around those values determined from Eq. (66) as n_ν decreases. This is true not only for the bipolar systems with $\theta_\nu \simeq \pi/2$ but also for those with other vacuum mixing angles.

The results shown in Fig. 3 can be understood as follows. Although Eqs. (3) and (46) are not equivalent over a long period for a time-varying n_ν , we may still view a bipolar system as a flavor pendulum over a short time interval during which n_ν does not change much. Suppose that at instant t_1 the flavor pendulum precesses uniformly around \mathbf{H}_V at latitude $\vartheta_0(t_1)$. In the adiabatic limit this precession continues as n_ν slowly changes, but the value of ϑ_0 changes with n_ν [ϑ_0 is a function of ϑ_1 and ϑ_2 which vary with n_ν according to Eq. (66)]. Of course, in realistic conditions, n_ν can only decrease with a finite rate, and the actual polar angle ϑ of the pendulum always “wobbles” (as a result of excitation of nutation modes) around ϑ_0 with some nutation period T_{nut} . However, if n_ν changes so slowly that

$$\left[T_{\text{nut}} \left(\frac{dn_\nu}{dt} \right) \right]^{-1} \gg \left(\frac{d\vartheta_0}{dn_\nu} \right), \left(\frac{\partial \vartheta}{\partial n_\nu} \right), \quad (67)$$

ϑ can be expected to closely follow ϑ_0 , and Eq. (66) becomes an excellent approximation. This expectation can be verified by comparing panels (b) and (d) of Fig. 3 where the evolution of two otherwise identical bipolar systems is calculated using different adiabatic parameters [$\gamma = 40$ in (b) and 200 in (d)]. With a much slower change in n_ν for panel (d), the result obtained by solving Eq. (66) becomes very close to that derived from the exact numerical calculations.

The final values of $\vartheta_1|_{n_\nu=0}$ and $\vartheta_2|_{n_\nu=0}$ of the bipolar system in the pure precession mode can be obtained as follows. The precession frequency Ω of the flavor pendulum cannot be 0, and therefore, cannot change sign as n_ν decreases. Because $\Omega = \Omega_{\text{sync}} > 0$ in the limit of large n_ν for $\alpha < 1$ [Eq. (62)], we have $\Omega > 0$. Eq. (65b) would give $\Omega > 0$ for $n_\nu = 0$ only if

$$\vartheta_2|_{n_\nu=0} = \pi. \quad (68)$$

This and Eq. (65) then give

$$\Omega|_{n_\nu=0} = \mu_V. \quad (69)$$

Combining Eqs. (68) and (66b) we obtain

$$\cos \vartheta_1|_{n_\nu=0} = (1 - \alpha) \cos 2\theta_\nu + \alpha. \quad (70)$$

This agrees with the numerical results shown in Fig. 3. For the inverted mass hierarchy scenario with $\theta_\nu \simeq \pi/2$, we have $\hat{\mathbf{e}}_z^f \simeq -\mathbf{H}_V$ and

$$P_{\nu_e \nu_e}|_{n_\nu=0} \simeq \frac{1 - \cos \vartheta_1}{2} \Big|_{n_\nu=0} \simeq 1 - \alpha, \quad (71a)$$

$$P_{\bar{\nu}_e \bar{\nu}_e}|_{n_\nu=0} \simeq \frac{1 + \cos \vartheta_2}{2} \Big|_{n_\nu=0} \simeq 0. \quad (71b)$$

However, we note that these results for $n_\nu = 0$ do not apply to realistic bipolar systems with finite spreads in the neutrino and antineutrino energy spectra as collective oscillations of these systems always break down before n_ν reaches 0.

B. Critical neutrino number density for the inverted mass hierarchy scenario with $\theta_\nu \simeq \pi/2$

In Fig. 3 one can see that, for the inverted mass hierarchy scenario with $\theta_\nu \simeq \pi/2$, \mathbf{s}_1 and \mathbf{s}_2 begin to misalign with \mathbf{H}_V when n_ν is smaller than some critical value n_ν^c , and there seems to be discontinuity in $d\vartheta_{1(2)}/dn_\nu$ at $n_\nu = n_\nu^c$. To understand these results, we consider the limit where $\theta_\nu = \pi/2$. We define

$$x_{1(2)} \equiv \sin \vartheta_{1(2)}. \quad (72)$$

For $\vartheta_1 \simeq \pi$ and $\vartheta_2 \simeq 0$ we have

$$\cos \vartheta_1 \simeq -1 + \frac{x_1^2}{2}, \quad (73a)$$

$$\cos \vartheta_2 \simeq 1 - \frac{x_2^2}{2}. \quad (73b)$$

Combining Eqs. (66) and (73) we obtain

$$4x_1x_2 \simeq (x_1 - \alpha x_2) \frac{n_\nu}{n_\nu^0} \times \left[x_2 \left(1 - \frac{x_1^2}{2} \right) - x_1 \left(1 - \frac{x_2^2}{2} \right) \right], \quad (74a)$$

$$1 - \alpha \simeq \left(1 - \frac{x_1^2}{2} \right) - \alpha \left(1 - \frac{x_2^2}{2} \right). \quad (74b)$$

Eq. (74) has the solution

$$x_1^2 \simeq \alpha x_2^2 \simeq 2\sqrt{\alpha} \left(\frac{n_\nu^c}{n_\nu} - 1 \right) \quad \text{if } n_\nu < n_\nu^c, \quad (75)$$

where

$$n_\nu^c \equiv \frac{4n_\nu^0}{(1 - \sqrt{\alpha})^2}. \quad (76)$$

Therefore, for the limiting case with $\theta_\nu = \pi/2$, \mathbf{s}_1 and \mathbf{s}_2 only start to misalign with \mathbf{H}_V when n_ν becomes smaller than n_ν^c .

One can also obtain the same value for n_ν^c from the gyroscopic flavor pendulum analogy using Eq. (52). For $\vartheta_{\text{max}} = \pi$, one always has $\vartheta_{\text{min}} = \pi$ if ⁴

$$\eta = \frac{\sigma^2}{4M^2g} > 1. \quad (77)$$

⁴ Ref. [24] pointed out the existence of the critical neutrino number density n_ν^c using this argument but gives $n_\nu^c \simeq n_\nu^x$.

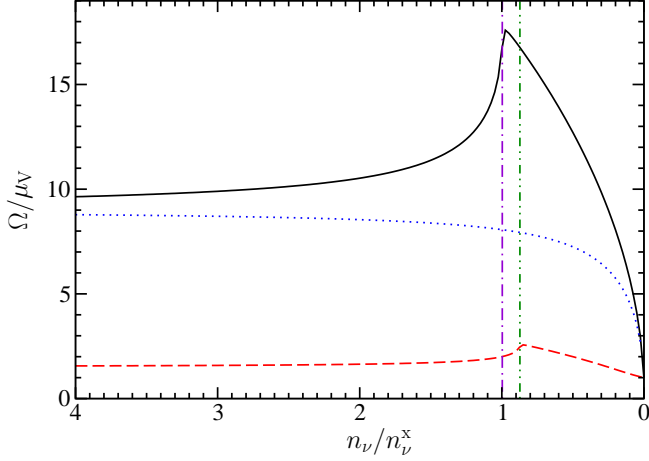


FIG. 4: (Color online) Scaled precession frequency Ω/μ_V of the flavor pendulum as a function of neutrino number density n_ν . The pendulum is assumed to be in the pure precession mode. The vacuum mixing angle is $\tilde{\theta}_v = 0.01$ for the solid and dashed lines, and $\theta_v = 0.6$ for the dotted line. The asymmetry parameter is $\alpha = 0.8$ for the solid and dotted lines and is 0.2 for the dashed line. The vertical dot-dashed line and dot-dot-dashed line correspond to $n_\nu = n_\nu^c$ for $\alpha = 0.8$ and 0.2, respectively.

Such a gyroscopic pendulum is known as a “sleeping top” because the pendulum “sleeps” in the upright position defying the effect of the gravity (see, *e.g.*, Ref. [32] for more discussions).

We note that the period of nutation T_{nut} of the flavor pendulum is infinite if $\theta_v = \pi/2$. For a symmetric bipolar system $T_{\text{nut}} \propto |\ln \tilde{\theta}_v|$ if $\theta_v \simeq \pi/2$ (see Sec. II A and also Ref. [24]). One expects similarly long nutation periods for asymmetric bipolar systems in the region where $n_\nu \simeq n_\nu^c$. In the same region, ϑ_1 and ϑ_2 change very quickly in the pure precession limit. As a result, the condition in Eq. (67) is usually violated in realistic environments and significant nutation can appear for $n_\nu < n_\nu^c$ [see, *e.g.*, Fig. 3(b)].

C. Precession frequency

Using Eq. (65) we have calculated the precession frequency Ω of the flavor pendulum for several scenarios assuming the pendulum is always in the pure precession mode. The results are plotted in Fig. 4. The precession frequency Ω asymptotically approaches the synchronization frequency Ω_{sync} in the synchronized regime ($n_\nu/n_\nu^x \gg 1$) as n_ν becomes larger and larger. On the other hand, Ω changes steeply with n_ν in the bipolar regime ($n_\nu/n_\nu^x \lesssim 1$). As n_ν reaches 0, $\Omega = \mu_V$ and the flavor pendulum precesses with the vacuum oscillation frequency of the dominant neutrino species (ν_e in this case).

We also note that, for the inverted mass hierarchy sce-

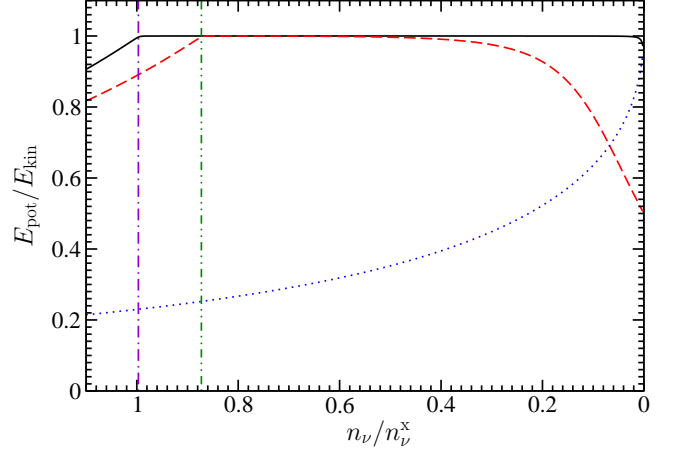


FIG. 5: (Color online) Ratio of the potential energy E_{pot} of the flavor pendulum to its kinetic energy E_{kin} [Eq. (49)] as functions of neutrino number density n_ν . The parameters and the meaning of the lines are the same as those in Fig. 4.

nario with $\theta_v \simeq \pi/2$, the precession frequency Ω reaches its maximum at $n_\nu \simeq n_\nu^c$. Using Eqs. (65) and (75), we obtain

$$\Omega|_{n_\nu=n_\nu^c} = 1 + \frac{2\sqrt{\alpha}}{1-\sqrt{\alpha}} \quad \text{for } \theta_v = \frac{\pi}{2}, \quad (78)$$

which is 17.9 for $\alpha = 0.8$ and 2.6 for $\alpha = 0.2$. These values agree well with the solid and dashed lines in Fig. 4 which assume $\tilde{\theta}_v = 0.01$.

D. Equipartition of energies?

Ref. [24] observed that, for $\theta_v \simeq \pi/2$, the total energy of a flavor pendulum begins to be approximately equipartitioned between its potential and kinetic energies when n_ν reaches n_ν^c . Using Eq. (75) one can show that (see Appendix), for the extreme case $\theta_v = \pi/2$, the ratio of energies is $E_{\text{pot}}/E_{\text{kin}} \simeq 1$ to $\mathcal{O}(n_\nu^c/n_\nu - 1)$ at $n_\nu \simeq n_\nu^c$ if the flavor pendulum stays in the pure precession mode.

Ref. [24] also mentioned “an important detail” that energy equipartition cannot hold all the way down to very small n_ν because E_{pot} has a finite positive minimum and E_{kin} ultimately reaches 0. This is illustrated in Fig. 8 of the same reference. However, we can show that (see Appendix)

$$\frac{E_{\text{pot}}}{E_{\text{kin}}} \simeq 1 - \frac{(1-\alpha)\cos^2 2\theta_v}{1+\alpha-2\alpha\cos 2\theta_v} \quad \text{for } \left(\frac{n_\nu}{n_\nu^0}\right) \ll 1 \quad (79)$$

if the flavor pendulum stays in the pure precession mode.

In Fig. 5 we plot the ratio $E_{\text{pot}}/E_{\text{kin}}$ as a function n_ν for three different bipolar systems in the pure precession mode with various choices of α and θ_v . Indeed, for the bipolar systems with $\theta_v \simeq \pi/2$, $E_{\text{pot}}/E_{\text{kin}}$ reaches 1 at $n_\nu = n_\nu^c$ and does not change much for a significant range

of n_ν . This is especially true for $\alpha \simeq 1$. In the limit $n_\nu = 0$, $E_{\text{pot}}/E_{\text{kin}} \simeq 0.94$ and 0.5 for $\theta_\nu \simeq \pi/2$ but $\alpha = 0.8$ and 0.2 , respectively. In the same limit, $E_{\text{pot}}/E_{\text{kin}} \simeq 0.98$ for $\theta_\nu = 0.6$ and $\alpha = 0.8$. These results agree well with Eq. (79).

V. NEUTRINO OSCILLATIONS IN SUPERNOVAE

Refs. [22, 23] have presented two sets of simulations using the “single-angle” and “multi-angle” approximations, respectively. These simulations together with the simple analytical and numerical models discussed in the previous sections represent approximations to the real supernova neutrino oscillation problem at three different levels of complexity.

The analytical and numerical calculations performed in this paper assume that the neutrino gas is homogeneous and isotropic and is represented by two mono-energetic neutrino and/or antineutrino species.

The single-angle simulations increase the complexity by allowing each neutrino species (4 in the 2×2 case) to have continuous energy distributions. It assumes that the flavor evolution histories of neutrinos propagating along different trajectories are the same as those of neutrinos emitted radially from the neutrino sphere. Although the single-angle approximation incorporates the angle dependence of neutrino-neutrino forward scattering into the “effective neutrino density” [22], it still assumes that neutrino on all trajectories evolve similarly.

The multi-angle simulations are by far the most sophisticated treatment of the problem. In these calculations neutrinos and antineutrinos have not only continuous energy distributions but also continuous angular distributions. The most important improvement implemented in the multi-angle simulations is that the flavor evolution of neutrinos and antineutrinos (with a wide range of energies) propagating along different trajectories is followed independently.

In this section we will first apply our simple models to the single-angle calculations. We will discuss the onset of neutrino flavor conversion in both the inverted and normal mass hierarchy scenarios (Secs. V A and V B). We will also investigate the precession mode of the neutrino gas in supernovae and its effects (Sec. V C). Finally, we will offer some new analyses of the multi-angle simulations and comment on the collectivity of neutrino flavor transformation in supernovae (Sec. V D).

A. Onset of neutrino flavor conversion in the inverted mass hierarchy scenario

The simulations presented in Refs. [22, 23] for the inverted neutrino mass hierarchy scenario all have $\hat{\theta}_\nu = 0.1$. According to the discussions in Sec. IV B, bipolar neutrino systems with vacuum mixing angle $\theta_\nu \simeq \pi/2$ can

start flavor conversion after the neutrino number density n_ν drops below some critical value n_ν^c . Although the conclusion was made in the absence of an ordinary matter background, it has been shown that the evolution of bipolar systems is not changed qualitatively even in a dominant matter background as long as $\theta_\nu \simeq \pi/2$ [21, 24].

For a rough estimate of the radius where $n_\nu = n_\nu^c$, we assume that the neutrino gas behaves in a way similar to the simple bipolar system initially consisting of ν_e and $\bar{\nu}_e$ with energies $E_{\nu_e} = 11$ MeV and $E_{\bar{\nu}_e} = 16$ MeV, respectively. (These values are the same as the average energies of ν_e and $\bar{\nu}_e$ in the simulations.) In a properly chosen corotating frame, the evolution of this simplified bipolar system is the same as that of a gas initial consisting of mono-energetic ν_e and $\bar{\nu}_e$ with energy [21]

$$\bar{E}_\nu \equiv \left[\frac{1}{2} \left(\frac{1}{E_{\nu_e}} + \frac{1}{E_{\bar{\nu}_e}} \right) \right]^{-1} \quad (80a)$$

$$\simeq 13 \text{ MeV}. \quad (80b)$$

With the luminosities of all neutrino species being the same and $L_\nu = 10^{51}$ erg/s, the ratio of the number densities of the two neutrino species is

$$\alpha = \frac{L_\nu/E_{\bar{\nu}_e}}{L_\nu/E_{\nu_e}} \simeq 0.69. \quad (81)$$

Therefore, the critical neutrino number density is [see Eq. (76)]

$$n_\nu^c = \frac{\delta m^2}{\sqrt{2} G_F \bar{E}_\nu} (1 - \sqrt{\alpha})^{-2} \quad (82a)$$

$$\simeq 6.24 \times 10^{28} \text{ cm}^{-3} \quad (82b)$$

for a mass squared difference $\delta m^2 = 3 \times 10^{-3} \text{ eV}^2$. Using the single-angle approximation we estimate the effective neutrino number density to be ⁵

$$n_\nu^{\text{eff}}(r) = \frac{L_\nu}{4\pi R_\nu^2 E_{\nu_e}} \left[1 - \sqrt{1 - \left(\frac{R_\nu}{r} \right)^2} \right]^2 \quad (83a)$$

$$\simeq (1.25 \times 10^{32} \text{ cm}^{-3}) \left[1 - \sqrt{1 - \left(\frac{R_\nu}{r} \right)^2} \right]^2, \quad (83b)$$

where $R_\nu = 11$ km is the radius of the neutrino sphere adopted in the simulation. Therefore, $n_\nu^{\text{eff}} \simeq n_\nu^c$ at radius $r_c \simeq 52$ km.

From panels (c) and (d) of Fig. 8 in Ref. [22] one sees that, in the single angle simulation, the flavor conversion starts at the radius $r_X \simeq 63$ km. At $r \gtrsim r_X$ the

⁵ Eq. (83) is similar to Eq. (40) in Ref. [22] except that we here are not computing the net effective neutrino density and, therefore, ignore the contribution of antineutrinos.

z -components of NFIS's \mathbf{s}_{ν_e} experience rapid oscillations which correspond to the nutation mode of the flavor pendulum. The estimated value of $r_c \simeq 52$ km and the observed value of $r_X \simeq 63$ km differ by ~ 10 km. This difference most likely arises because at $r \simeq r_c$ the nutation frequency T_{nut}^{-1} of the flavor pendulum is very small. Consequently, there is a delay before significant nutation amplitude can develop. On the other hand, smaller nutation frequency implies less adiabatic evolution [see Eq. (67)]. So once developed, the nutation amplitude will be large. The oscillation amplitudes of $\langle s_{\nu_e z} \rangle$ and $\langle s_{\bar{\nu}_e z} \rangle$ are indeed large as shown in Fig. 8 of Ref. [22].

We note that the region ($r_c \lesssim r \lesssim r_X$) where the nutation modes are to be excited is roughly the same region where the chaos-like phenomenon shown in Fig. 12 of Ref. [22] occurs. In this region the differences of two almost identical systems can grow exponentially as they evolve.

B. Onset of neutrino flavor conversion in the normal mass hierarchy scenario

The simulations presented in Refs. [22, 23] for the normal neutrino mass hierarchy scenario all have $\theta_v = 0.1$. According to the discussions in Sec. III, a bipolar neutrino system with vacuum mixing angle $\theta_v \ll 1$ corresponds to a flavor pendulum that oscillates in a very limited region near the bottom of the potential well, and therefore, does not experience much flavor transformation. However, this conclusion only applies in the absence of an ordinary matter background.

In the presence of a matter background, it has been shown that, in the synchronized regime, neutrinos and antineutrinos of all the species and energies go through an MSW-like resonance simultaneously in the same way as does a neutrino with the characteristic energy E_{sync} in the conventional MSW picture [18]. A similar phenomenon may also occur in bipolar systems in the bipolar regime (*i.e.*, outside the synchronized regime) as suggested in Ref. [21]. If this is true, the dominant neutrino species are changed from ν_e and $\bar{\nu}_e$ to $\nu_{\mu,\tau}$ and $\bar{\nu}_{\mu,\tau}$. Using the corotating frame, one can show that the evolution of a $\bar{\nu}_{\mu,\tau}$ - $\nu_{\mu,\tau}$ gas with the normal mass hierarchy is similar to that of a ν_e - $\bar{\nu}_e$ gas with the inverted mass hierarchy [21], and the flavor pendulum is raised from the bottom position to the top position because of the change in the dominant neutrino species. Bipolar systems can subsequently develop nutation modes after the collective MSW-like resonance.

From panels (a) and (b) of Fig. 8 in Ref. [22] one sees that, in the single angle simulation, the z -components of NFIS's \mathbf{s}_{ν_e} suddenly change at radius $r_X \simeq 88$ km and oscillate rapidly afterwards. This corresponds to the initial collective MSW-like resonance followed by the nutation modes. We note that the observed value of r_X in the simulation is larger than the value of 74 km estimated for the fully synchronized limit [22]. The difference arises partly

because the MSW-like resonance actually occurs in the bipolar regime in this case.

C. Precession mode and final neutrino survival probabilities

As shown in Sec. III bipolar systems generally are in both precession and nutation modes. This is indeed seen in the single-angle simulations for both the normal and inverted mass hierarchies. In Fig. 8 of Ref. [22], the x - and y -components of NFIS's \mathbf{s}_{ν_e} oscillate with an approximate phase difference of $\pi/2$, signifying precession in the x - y plane.

In Sec. IV A we have argued that, in the absence of an ordinary matter background, the intrinsic precession angular velocity $\mathbf{\Omega}$ of the bipolar system as a whole should be in the same direction as that of a single neutrino of the dominant species. Therefore, we expect bipolar systems dominated by neutrinos to tend to precess around $-\mathbf{H}_V$. In the presence of a matter background, bipolar systems will also tend to precess around the direction opposite to

$$\mathbf{H}_e \equiv -\hat{\mathbf{e}}_z^f \sqrt{2} G_F n_e, \quad (84)$$

where n_e is the net electron number density. For the inverted mass hierarchy with $\theta_v \simeq \pi/2$ and $\mathbf{H}_V \simeq -\hat{\mathbf{e}}_z^f$, the intrinsic $\mathbf{\Omega}$ of the flavor pendulum is roughly in the same direction as the precession stemming from the matter background. In this case, the combined precession does not change direction. As a result, the precession of NFIS's is always roughly around $-\mathbf{H}_V \simeq \hat{\mathbf{e}}_z^f$ for the inverted mass hierarchy.

For the normal mass hierarchy with $\theta_v \ll 1$ and $\mathbf{H}_V \simeq \hat{\mathbf{e}}_z^f$, the intrinsic $\mathbf{\Omega}$ of the flavor pendulum is roughly in the opposite direction to that of the precession due to the matter background, and the combined precession may change its direction. However, it is expected that the matter background becomes negligible after the collective MSW-like resonance. Therefore, the NFIS's precess roughly in the direction of $-\mathbf{H}_V \simeq -\hat{\mathbf{e}}_z^f$ in the region $r \gtrsim r_X$ for the normal mass hierarchy. According to Fig. 8 of Ref. [22] NFIS's indeed precess around $\hat{\mathbf{e}}_z^f$ for the inverted mass hierarchy scenario and $-\hat{\mathbf{e}}_z^f$ for the normal mass hierarchy scenario.

Ref. [22] has shown that (see Fig. 9 of that reference), for the inverted mass hierarchy scenario and at large radius, neutrinos with energies below $E_C \simeq 9$ MeV are mostly in their initial flavors while neutrinos with larger energies and most antineutrinos can be completely converted to other flavors in the limit of large neutrino luminosity L_ν . For the normal mass hierarchy scenario, neutrinos with energies below $E_C \simeq 9$ MeV are almost completely converted to other flavors while neutrinos with larger energies and nearly all antineutrinos are mostly in their initial flavors in the limit of large L_ν . Ref. [22] suggested that this phenomenon is related to the precession of NFIS's when neutrino number densities decrease

and the bipolar configuration starts to break down (see Fig. 10 of that reference).

We note that the precession of NFIS's due to the matter background \mathbf{H}_e is the same for all neutrinos, and we can essentially ignore it in a reference frame \mathcal{F}_1 rotating with angular velocity $-\mathbf{H}_e$. In this corotating frame \mathcal{F}_1 , the e.o.m. of NFIS \mathbf{s}_i is

$$\frac{d}{dt}\mathbf{s}_i = \mathbf{s}_i \times \mathbf{H}_{\text{tot}} \quad (85a)$$

$$\equiv \mathbf{s}_i \times (\mu_{V,i}\mathbf{H}_V + \mathbf{H}_\nu) \quad (85b)$$

$$\equiv \mathbf{s}_i \times (\mu_{V,i}\mathbf{H}_V + \mu_\nu \sum_j n_{\nu,j}\mathbf{s}_j) \quad (85c)$$

where \mathbf{H}_ν is the effective “magnetic field” generated by all other NFIS's. We assume that all NFIS's and \mathbf{H}_ν rotate with a constant angular velocity $-\Omega\mathbf{H}_V$. The problem becomes very simple in a reference frame \mathcal{F}_2 which rotates relative to \mathcal{F}_1 with angular velocity $-\Omega\mathbf{H}_V$. In \mathcal{F}_2

$$\frac{d}{dt}\mathbf{s}_i = \mathbf{s}_i \times \tilde{\mathbf{H}}_{\text{tot}} \quad (86a)$$

$$\equiv \mathbf{s}_i \times [(\mu_{V,i} - \Omega)\mathbf{H}_V + \tilde{\mathbf{H}}_\nu], \quad (86b)$$

where both $\tilde{\mathbf{H}}_{\text{tot}}$ and $\tilde{\mathbf{H}}_\nu$ are not rotating⁶.

We first look at a NFIS \mathbf{s}_i corresponding to a neutrino which is initially pure ν_e at the neutrino sphere. Because $\mu_\nu \equiv -2\sqrt{2}G_F$ is negative and the neutrino gas is initially dominated by ν_e , the NFIS \mathbf{s}_i must be roughly antialigned with $\tilde{\mathbf{H}}_{\text{tot}} \simeq \tilde{\mathbf{H}}_\nu$ when neutrino number densities are large. As neutrino number densities decrease to 0, $\tilde{\mathbf{H}}_{\text{tot}} \rightarrow (\mu_{V,i} - \Omega)\mathbf{H}_V$. If neutrino number densities decrease so slowly that the process is adiabatic, \mathbf{s}_i will stay antialigned with $\tilde{\mathbf{H}}_{\text{tot}}$. At $n_\nu = 0$ the NFIS \mathbf{s}_i can be either aligned or antialigned with \mathbf{H}_V depending on whether $\mu_{V,i}$ is smaller or larger than Ω . For the inverted mass hierarchy scenario with $\theta_\nu \simeq \pi/2$ and $\mathbf{H}_V \simeq -\hat{\mathbf{e}}_z^f$, \mathbf{s}_i is roughly aligned with $\hat{\mathbf{e}}_z^f \simeq -\mathbf{H}_V$ if $\mu_V \equiv \delta m^2/(2E_\nu) > \Omega$ and antialigned with $\hat{\mathbf{e}}_z^f$ otherwise. Accordingly, at large radii neutrinos starting as ν_e are still mostly in the ν_e flavor if their energies are below

$$E_C \equiv \frac{\delta m^2}{2\Omega} \quad (87)$$

and are almost completely converted to other flavors otherwise. In words, one has

$$P_{\nu\nu}(E_\nu) \simeq \begin{cases} 1 & \text{if } E_\nu < E_C, \\ 0 & \text{if } E_\nu > E_C. \end{cases} \quad (88)$$

⁶ We have ignored the rotation of \mathbf{H}_V in the corotating frames \mathcal{F}_1 and \mathcal{F}_2 because \mathbf{H}_V is roughly in the same or opposite direction as the rotation axis for $\theta_\nu \ll 1$ or $\theta_\nu \simeq \pi/2$.

TABLE I: Final neutrino survival probabilities in the adiabatic limit for large L_ν in both the normal and inverted neutrino mass hierarchy scenarios.

	$\theta_\nu \ll 1$ (normal)	$\theta_\nu \simeq \pi/2$ (inverted)
$P_{\nu\nu}(E_\nu < E_C)$	0	1
$P_{\nu\nu}(E_\nu > E_C)$	1	0
$P_{\bar{\nu}\bar{\nu}}(E_{\bar{\nu}})$	1	0

One can estimate the final neutrino survival probabilities for other cases in a similar fashion. We have summarized the results for the relevant scenarios in Table I.

In this analysis we have assumed Ω to be constant. This analysis is expected to hold as long as the process is more or less adiabatic and neutrino number densities decrease slowly. The predictions from this simple analysis generally agree with the results of single-angle numerical simulations presented in Fig. 9 of Ref. [22]. The agreement is especially good for large neutrino luminosities and in the neutrino sector for which $P_{\nu\nu}(E_\nu)$ has a relatively sharp transition or jump at $E_\nu \simeq E_C$. This pattern can be taken as a hallmark of collective neutrino flavor transformation because it results from a neutrino background that is in a collective precession mode.

D. Collectivity and non-collectivity of neutrino oscillations in supernovae

Single-angle simulations assumed that neutrinos of the same species and energy all evolve in the same way even if they are emitted in different angles from the neutrino sphere. This is not necessarily always a good approximation as neutrino-neutrino forward scattering is angle dependent and the neutrino density distributions in the supernova environment are inhomogeneous and anisotropic. Even if neutrinos moving along various trajectories all have the same flavor content at a given radius, they produce different refractive indices for neutrinos propagating in different directions. Therefore, neutrinos propagating in different directions are expected to have different flavor evolution histories. On the other hand, neutrinos propagating along different trajectories are coupled to each other through neutrino-neutrino forward scattering. The correlations among different neutrino trajectories are especially strong when neutrino fluxes are large. The inhomogeneity/anisotropy of the environment and the correlation among different neutrino trajectories act as two opposite “forces” which try to break and uphold, respectively, the collective aspect of neutrino oscillations in supernovae. At the moment it is difficult to perform an analytical study that can clearly predict which force wins. Our limited goal here is to gain insight into the issue of collectivity of neutrino flavor transformation by analyzing the multi-angle simulations presented in Refs. [22, 23].

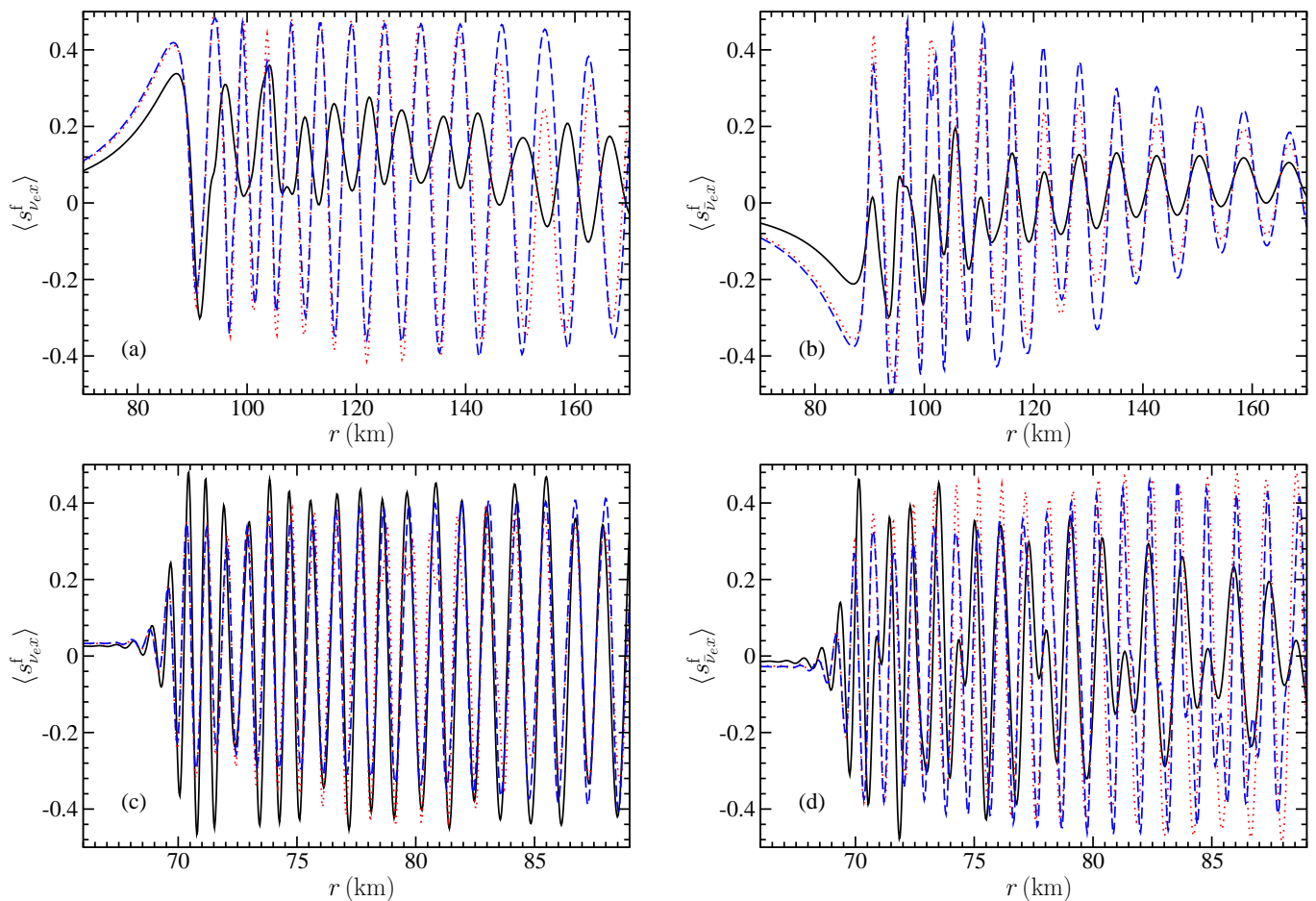


FIG. 6: (Color online) The evolution of x -components of the average NFIS's of supernova neutrinos in the flavor basis obtained from the multi-angle simulations as presented in Fig. 4 of Ref. [22]. The left panels are for neutrinos emitted as ν_e , and the right panels are for antineutrinos emitted as $\bar{\nu}_e$. The top panels employ the normal mass hierarchy with $\theta_v = 0.1$, and the bottom panels employ the inverted mass hierarchy with $\theta_v = 0.1$. The solid, dotted and dashed lines give $\langle s_{\nu_e x}^f \rangle$ along the trajectories with $\cos \Theta_0 = 1, 0.5$ and 0 , respectively, where Θ_0 is the emission angle defined in Ref. [22]. The neutrino mass-squared difference is taken to be $\delta m^2 = 3 \times 10^{-3} \text{ eV}^2$.

As shown in Fig. 2 of Ref. [23], the flavor evolution of neutrinos on each trajectory in multi-angle simulations looks qualitatively similar to that in the corresponding single-simulations. However, the oscillations in neutrino survival probabilities $P_{\nu\nu}$ and $P_{\bar{\nu}\bar{\nu}}$ have different frequencies for different trajectories. For vacuum angle $\theta_v \ll 1$ or $\theta_v \simeq \pi/2$, the oscillations in $P_{\nu\nu}$ and $P_{\bar{\nu}\bar{\nu}}$ represent the nutation of the flavor pendulum. Therefore, the nutation modes of neutrinos propagating along different trajectories cannot be viewed as collective. Indeed, it has recently been shown that the nutation modes for symmetric bipolar systems can quickly develop large phase differences and “de-cohere” for neutrinos propagating in different directions [26].

On the other hand, Fig. 3 of Ref. [23] shows that $P_{\nu\nu}(E_\nu)$ obtained by multi-angle simulations has a sharp transition at $E_\nu = E_C$ as in single-angle simulations. In addition, the value of E_C is approximately independent

of neutrino trajectory direction. If this transition is related to the precession mode of neutrinos as suggested by Ref. [22] and further explained here, NFIS's corresponding to neutrinos propagating in different directions must precess with the same frequency. In Fig. 6 we have plotted $\langle s_{\nu_e x}^f \rangle$, the x -component of the average NFIS's in the flavor basis, as functions of radius r for three representative trajectories obtained from the multi-angle simulations of Refs. [22, 23]. One indeed observes that the NFIS's along various trajectories are approximately in a single collective precession mode and precess around $\pm \hat{\mathbf{e}}_z$ with approximately the same frequency.

VI. CONCLUSIONS

We have investigated the simple symmetric bipolar system using the flavor pendulum analogy. We have shown

that an adiabatic invariant of the pendulum motion can be used to study the evolution of such a bipolar system when neutrino number densities change slowly with time. We have also studied an asymmetric bipolar system using the gyroscopic pendulum analogy. As a gyroscopic pendulum, a bipolar system generally can be in both the precession and nutation modes simultaneously except in the synchronized regime where only precession is possible.

We have shown that an asymmetric bipolar system can stay mostly in a pure precession mode as it transitions from the synchronized regime into the bipolar regime if neutrino number densities decrease slowly. The precession frequency of the system generally varies with the neutrino number density and approaches the synchronization frequency in the synchronized regime. For the inverted mass hierarchy case with mixing angle $\theta_v \simeq \pi/2$, we have calculated a more accurate value of the critical neutrino number density below which bipolar systems can start flavor transformation. Because supernova neutrinos naturally form asymmetric bipolar systems, these analyses could be useful for understanding the qualitative features of neutrino oscillations in supernovae.

We have further analyzed the recent numerical simulations of neutrino oscillations in supernovae. These large-scale simulations suggest that neutrinos traveling on intersecting trajectories and experiencing destructive quantum interference nevertheless can be in the collective precession mode. This mode can result in sharp transitions in the final energy-dependent neutrino survival probabilities $P_{\nu\nu}(E_\nu)$ across all trajectories. This sharp transition in $P_{\nu\nu}(E_\nu)$ can be taken as a hallmark of collective neutrino flavor transformation. Moreover, this transition occurs differently for the normal and inverted neutrino mass hierarchies. Based on this difference, the

neutrino signals from a future galactic supernova potentially can be used to determine the actual neutrino mass hierarchy.

APPENDIX: POTENTIAL AND KINETIC ENERGIES OF AN ASYMMETRIC FLAVOR PENDULUM

Let us compare the kinetic energy E_{kin} of the flavor pendulum with its potential energy E_{pot} [see Eq. (49)] in the pure precession mode. The potential energy is defined as

$$E_{\text{pot}} \equiv Mg(1 - \mathbf{H}_V \cdot \mathbf{r}) = \mu_V(q - \mathbf{q} \cdot \mathbf{H}_V), \quad (\text{A.1})$$

where

$$\mathbf{q} \equiv \frac{\mathbf{Q}}{n_\nu} = \mathbf{s}_1 - \alpha \mathbf{s}_2 + \frac{n_\nu^0}{n_\nu} \mathbf{H}_V. \quad (\text{A.2})$$

Its kinetic energy is defined as

$$E_{\text{kin}} \equiv \frac{\mathbf{J}^2}{2M} = \frac{\mu_V}{2} \left(\frac{n_\nu}{n_\nu^0} \right) \mathbf{J}^2, \quad (\text{A.3})$$

where

$$\mathbf{J} \equiv \mathbf{s}_1 + \alpha \mathbf{s}_2. \quad (\text{A.4})$$

According to Eq. (75), we have $\sin^2 \vartheta_1 \simeq \alpha \sin^2 \vartheta_2$ and $\sin^2 \vartheta_2 \simeq 2\delta/\sqrt{\alpha}$ if

$$\delta \equiv \frac{n_\nu^c}{n_\nu} - 1 \ll 1. \quad (\text{A.5})$$

It is straightforward to show that

$$q = \sqrt{(\mathbf{s}_1 - \alpha \mathbf{s}_2)^2 + 2 \left(\frac{n_\nu^0}{n_\nu} \right) (\mathbf{s}_1 \cdot \mathbf{H}_V - \alpha \mathbf{s}_2 \cdot \mathbf{H}_V) + \left(\frac{n_\nu^0}{n_\nu} \right)^2} \quad (\text{A.6a})$$

$$= \sqrt{\frac{1 + \alpha^2 - 2\alpha \cos(\vartheta_1 + \vartheta_2)}{4} + \left(\frac{n_\nu^0}{n_\nu} \right) (\cos \vartheta_1 - \alpha \cos \vartheta_2) + \left(\frac{n_\nu^0}{n_\nu} \right)^2} \quad (\text{A.6b})$$

$$= \frac{1 + \alpha}{2} - \frac{n_\nu^0}{n_\nu} + \mathcal{O}(\delta^2). \quad (\text{A.6c})$$

In addition, we have

$$\mathbf{q} \cdot \mathbf{H}_V = \mathbf{s}_1 \cdot \mathbf{H}_V - \alpha \mathbf{s}_2 \cdot \mathbf{H}_V + \frac{n_\nu^0}{n_\nu} \quad (\text{A.7a})$$

$$\simeq -\frac{1 + \alpha}{2} + \frac{n_\nu^0}{n_\nu} + \sqrt{\alpha} \delta. \quad (\text{A.7b})$$

Combining Eqs. (A.6c) and (A.7b), we obtain

$$E_{\text{pot}} \simeq \mu_V \left[1 + \alpha - 2 \left(\frac{n_\nu^0}{n_\nu} \right) - \sqrt{\alpha} \delta \right] \quad (\text{A.8a})$$

$$= \mu_V \left[\frac{(1 + \sqrt{\alpha})^2}{2} - \left(\frac{1 + \alpha}{2} \right) \delta \right]. \quad (\text{A.8b})$$

Similarly, we have

$$\mathbf{J}^2 = \frac{1 + \alpha^2 + 2\alpha \cos(\vartheta_1 + \vartheta_2)}{4} \quad (\text{A.9a})$$

$$\simeq \left(\frac{1 - \alpha}{2}\right)^2 + \frac{\sqrt{\alpha}(1 - \sqrt{\alpha})^2}{2}\delta, \quad (\text{A.9b})$$

and

$$E_{\text{kin}} \simeq \frac{\mu_V}{1 + \delta} \left[\frac{(1 + \sqrt{\alpha})^2}{2} + \sqrt{\alpha}\delta \right] \quad (\text{A.10a})$$

$$\simeq \mu_V \left[\frac{(1 + \sqrt{\alpha})^2}{2} - \left(\frac{1 + \alpha}{2}\right)\delta \right]. \quad (\text{A.10b})$$

Therefore, we obtain $E_{\text{pot}}/E_{\text{kin}} \simeq 1$ to $\mathcal{O}(\delta)$ in the limit $\delta \ll 1$.

One can also estimate the potential and kinetic energies of the flavor pendulum in the limit $n_\nu/n_\nu^0 \ll 1$. In this limit we have $\mathbf{s}_1 \cdot \mathbf{H}_V \simeq \cos \vartheta_1/2$, $\mathbf{s}_2 \cdot \mathbf{H}_V \simeq -1/2$, and $\mathbf{s}_1 \cdot \mathbf{s}_2 \simeq -\cos \vartheta_1/4$. Therefore,

$$q = \sqrt{(\mathbf{s}_1 - \alpha \mathbf{s}_2)^2 + 2 \left(\frac{n_\nu^0}{n_\nu}\right) (\mathbf{s}_1 \cdot \mathbf{H}_V - \alpha \mathbf{s}_2 \cdot \mathbf{H}_V) + \left(\frac{n_\nu^0}{n_\nu}\right)^2} \quad (\text{A.11a})$$

$$= \left(\frac{n_\nu^0}{n_\nu}\right) \sqrt{1 + 2 \left(\frac{n_\nu}{n_\nu^0}\right) (\mathbf{s}_1 \cdot \mathbf{H}_V - \alpha \mathbf{s}_2 \cdot \mathbf{H}_V) + \left(\frac{n_\nu}{n_\nu^0}\right)^2 (\mathbf{s}_1 - \alpha \mathbf{s}_2)^2} \quad (\text{A.11b})$$

$$\simeq \frac{n_\nu^0}{n_\nu} + \mathbf{s}_1 \cdot \mathbf{H}_V - \alpha \mathbf{s}_2 \cdot \mathbf{H}_V + \frac{1}{2} \left(\frac{n_\nu}{n_\nu^0}\right) [(\mathbf{s}_1 - \alpha \mathbf{s}_2)^2 - (\mathbf{s}_1 \cdot \mathbf{H}_V - \alpha \mathbf{s}_2 \cdot \mathbf{H}_V)^2] \quad (\text{A.11c})$$

$$\simeq \mathbf{q} \cdot \mathbf{H}_V + \left(\frac{n_\nu}{n_\nu^0}\right) \frac{\sin^2 \vartheta_1}{8}, \quad (\text{A.11d})$$

which gives

$$E_{\text{pot}} \simeq \frac{\mu_V}{8} \left(\frac{n_\nu}{n_\nu^0}\right) \sin^2 \vartheta_1. \quad (\text{A.12})$$

Similary, we have

$$E_{\text{kin}} = \frac{\mu_V}{2} \left(\frac{n_\nu}{n_\nu^0}\right) (\mathbf{s}_1 + \alpha \mathbf{s}_2)^2 \quad (\text{A.13a})$$

$$\simeq \frac{\mu_V}{8} \left(\frac{n_\nu}{n_\nu^0}\right) (1 + \alpha^2 - 2\alpha \cos \vartheta_1). \quad (\text{A.13b})$$

Combining Eqs. (A.12) and (A.13b), we obtain

$$\frac{E_{\text{pot}}}{E_{\text{kin}}} \simeq \frac{\sin^2 \vartheta_1}{1 + \alpha^2 - 2\alpha \cos \vartheta_1}. \quad (\text{A.14})$$

In the limit $n_\nu/n_\nu^0 \ll 1$, $\cos \vartheta_1 \simeq (1 - \alpha) \cos 2\theta_v + \alpha$, and the above equation reduces to

$$\frac{E_{\text{pot}}}{E_{\text{kin}}} \simeq 1 - \frac{(1 - \alpha) \cos^2 2\theta_v}{1 + \alpha - 2\alpha \cos 2\theta_v}. \quad (\text{A.15})$$

ACKNOWLEDGMENTS

This work was supported in part by NSF grant PHY-04-00359, the TSI collaboration's DOE SciDAC grant at UCSD, and DOE grant DE-FG02-87ER40328 at UMN. This work was also supported in part by the LDRD Program and Open Supercomputing at LANL, and by the National Energy Research Scientific Computing Center through the TSI collaboration using Bassi, and the San Diego Supercomputer Center through the Academic Associates Program using DataStar. We would like to thank A. Friedland, T. Goldman, J. Hidaka and M. Patel for valuable conversations.

[1] Y. Z. Qian and G. M. Fuller, Phys. Rev. **D51**, 1479 (1995), astro-ph/9406073.

[2] Y.-Z. Qian, G. M. Fuller, G. J. Mathews, R. W. Mayle, J. R. Wilson, and S. E. Woosley, Phys. Rev. Lett. **71**,

- 1965 (1993).
- [3] G. M. Fuller, R. W. Mayle, B. S. Meyer, and J. R. Wilson, *Astrophys. J.* **389**, 517 (1992).
 - [4] G. M. Fuller, R. W. Mayle, J. R. Wilson, and D. N. Schramm, *Astrophys. J.* **322**, 795 (1987).
 - [5] J. T. Pantaleone, *Phys. Rev.* **D46**, 510 (1992).
 - [6] G. Sigl and G. Raffelt, *Nucl. Phys.* **B406**, 423 (1993).
 - [7] S. Samuel, *Phys. Rev.* **D48**, 1462 (1993).
 - [8] V. A. Kosteletzky and S. Samuel, *Phys. Rev.* **D49**, 1740 (1994).
 - [9] V. A. Kosteletzky, J. T. Pantaleone, and S. Samuel, *Phys. Lett.* **B315**, 46 (1993).
 - [10] V. A. Kosteletzky and S. Samuel, *Phys. Lett.* **B318**, 127 (1993).
 - [11] V. A. Kosteletzky and S. Samuel, *Phys. Rev.* **D52**, 621 (1995), hep-ph/9506262.
 - [12] S. Samuel, *Phys. Rev.* **D53**, 5382 (1996), hep-ph/9604341.
 - [13] V. A. Kosteletzky and S. Samuel, *Phys. Lett.* **B385**, 159 (1996), hep-ph/9610399.
 - [14] S. Pastor, G. G. Raffelt, and D. V. Semikoz, *Phys. Rev.* **D65**, 053011 (2002), hep-ph/0109035.
 - [15] A. D. Dolgov et al., *Nucl. Phys.* **B632**, 363 (2002), hep-ph/0201287.
 - [16] Y. Y. Y. Wong, *Phys. Rev.* **D66**, 025015 (2002), hep-ph/0203180.
 - [17] K. N. Abazajian, J. F. Beacom, and N. F. Bell, *Phys. Rev.* **D66**, 013008 (2002), astro-ph/0203442.
 - [18] S. Pastor and G. Raffelt, *Phys. Rev. Lett.* **89**, 191101 (2002), astro-ph/0207281.
 - [19] A. B. Balantekin and H. Yüksel, *New J. Phys.* **7**, 51 (2005), astro-ph/0411159.
 - [20] G. M. Fuller and Y.-Z. Qian, *Phys. Rev.* **D73**, 023004 (2006), astro-ph/0505240.
 - [21] H. Duan, G. M. Fuller, and Y.-Z. Qian, *Phys. Rev.* **D74**, 123004 (2005), astro-ph/0511275.
 - [22] H. Duan, G. M. Fuller, J. Carlson, and Y.-Z. Qian, *Phys. Rev.* **D74**, 105014 (2006), astro-ph/0606616.
 - [23] H. Duan, G. M. Fuller, J. Carlson, and Y.-Z. Qian, *Phys. Rev. Lett.* **97**, 241101 (2006), astro-ph/0608050.
 - [24] S. Hannestad, G. G. Raffelt, G. Sigl, and Y. Y. Y. Wong, *Phys. Rev.* **D74**, 105010 (2006), astro-ph/0608695.
 - [25] A. B. Balantekin and Y. Pehlivan, *J. Phys.* **G34**, 47 (2007), astro-ph/0607527.
 - [26] G. G. Raffelt and G. G. R. Sigl (2007), hep-ph/0701182.
 - [27] L. Wolfenstein, *Phys. Rev.* **D17**, 2369 (1978).
 - [28] L. Wolfenstein, *Phys. Rev.* **D20**, 2634 (1979).
 - [29] S. P. Mikheyev and A. Y. Smirnov, *Yad. Fiz.* **42**, 1441 (1985), [*Sov. J. Nucl. Phys.* **42**, 913 (1985)].
 - [30] L. D. Landau and E. M. Lifshitz, *Mechanics* (Pergamon, Oxford, 1976), 3rd ed.
 - [31] I. S. Gradshteyn and I. M. Ryzhik, *Table of integrals, series, and products* (Academic, Boston, 1994), 5th ed.
 - [32] J. B. Scarborough, *The Gyroscope, Theory and Application* (Interscience, New York, 1958).